EBNA3B-deficient EBV promotes B cell lymphomagenesis in humanized mice and is found in human tumors

White, Robert E ; Rämer, Patrick C ; Naresh, Kikkeri N ; Meixlsperger, Sonja ; Pinaud, Laurie ; Rooney, Cliona ; Savoldo, Barbara ; Coutinho, Rita ; Bödör, Csaba ; Gribben, John ; Ibrahim, Hazem A ; Bower, Mark ; Nourse, Jamie P ; Gandhi, Maher K ; Middeldorp, Jaap ; Cader, Fathima Z ; Murray, Paul ; Münz, Christian ; Allday, Martin J

Abstract: Epstein-Barr virus (EBV) persistently infects more than 90% of the human population and is etiologically linked to several B cell malignancies, including Burkitt lymphoma (BL), Hodgkin lymphoma (HL), and diffuse large B cell lymphoma (DLBCL). Despite its growth transforming properties, most immune-competent individuals control EBV infection throughout their lives. EBV encodes various oncogenes, and of the 6 latency-associated EBV-encoded nuclear antigens, only EBNA3B is completely dispensable for B cell transformation in vitro. Here, we report that infection with EBV lacking EBNA3B leads to aggressive, immune-evading monomorphic DLBCL-like tumors in NOD/SCID/ c-/- mice with reconstituted human immune system components. Infection with EBNA3B-knockout EBV (EBNA3BKO) induced expansion of EBV-specific T cells that failed to infiltrate the tumors. EBNA3BKO-infected B cells expanded more rapidly and secreted less T cell-chemoattractant CXCL10, reducing T cell recruitment in vitro and T cell-mediated killing in vivo. B cell lines from 2 EBV-positive human lymphomas encoding truncated EBNA3B exhibited gene expression profiles and phenotypic characteristics similar to those of tumor-derived lines from the humanized mice, including reduced CXCL10 secretion. Screening EBV-positive DLBCL, HL, and BL human samples identified additional EBNA3B mutations. Thus, EBNA3B is a virus-encoded tumor suppressor whose inactivation promotes immune evasion and virus-driven lymphomagenesis.

DOI: https://doi.org/10.1172/JCI58092

EBNA3B-deficient EBV promotes B cell lymphomagenesis in humanized mice and is found in human tumors

Robert E. White,[1] Patrick C. Rämer,[2] Kikkeri N. Naresh,[3] Sonja Meixlsperger,[2] Laurie Pinaud,[1] Cliona Rooney,[4] Barbara Savoldo,[4] Rita Coutinho,[5] Csaba Bödör,[5] John Gribben,[5] Hazem A. Ibrahim,[3] Mark Bower,[6] Jamie P. Nourse,[7] Maher K. Gandhi,[7] Jaap Middeldorp,[8] Fathima Z. Cader,[9] Paul Murray,[9] Christian Münz,[2] and Martin J. Allday[1]

[1]Section of Virology, Faculty of Medicine, Imperial College London, London, United Kingdom. [2]Viral Immunobiology, Institute of Experimental Immunology, University of Zürich, Zürich, Switzerland. [3]Department of Histopathology, Hammersmith Hospital Campus, Imperial College Healthcare NHS Trust, London, United Kingdom. [4]Center for Cell and Gene Therapy, Baylor College of Medicine, Houston, Texas, USA. [5]Centre of Haemato-Oncology, Barts Cancer Institute, Queen Mary University of London, London, United Kingdom. [6]Department of Medical Oncology, Chelsea and Westminster Hospital, London, United Kingdom. [7]Clinical Immunohaematology, Queensland Institute of Medical Research, Brisbane, Queensland, Australia. [8]Department of Pathology, VU University Medical Centre, Amsterdam, The Netherlands. [9]School of Cancer Sciences, College of Medical and Dental Sciences, University of Birmingham, Birmingham, United Kingdom.

Epstein-Barr virus (EBV) persistently infects more than 90% of the human population and is etiologically linked to several B cell malignancies, including Burkitt lymphoma (BL), Hodgkin lymphoma (HL), and diffuse large B cell lymphoma (DLBCL). Despite its growth transforming properties, most immune-competent individuals control EBV infection throughout their lives. EBV encodes various oncogenes, and of the 6 latency-associated EBV-encoded nuclear antigens, only EBNA3B is completely dispensable for B cell transformation in vitro. Here, we report that infection with EBV lacking EBNA3B leads to aggressive, immune-evading monomorphic DLBCL-like tumors in NOD/SCID/$\gamma_c^{-/-}$ mice with reconstituted human immune system components. Infection with EBNA3B-knockout EBV (EBNA3BKO) induced expansion of EBV-specific T cells that failed to infiltrate the tumors. EBNA3BKO-infected B cells expanded more rapidly and secreted less T cell–chemoattractant CXCL10, reducing T cell recruitment in vitro and T cell–mediated killing in vivo. B cell lines from 2 EBV-positive human lymphomas encoding truncated EBNA3B exhibited gene expression profiles and phenotypic characteristics similar to those of tumor-derived lines from the humanized mice, including reduced CXCL10 secretion. Screening EBV-positive DLBCL, HL, and BL human samples identified additional *EBNA3B* mutations. Thus, EBNA3B is a virus-encoded tumor suppressor whose inactivation promotes immune evasion and virus-driven lymphomagenesis.

Introduction

EBV is a ubiquitous γ-herpesvirus, persistently infecting more than 90% of the human adult population (1). Despite its growth transforming properties, the immune system of most individuals controls infection and helps prevent tumor development. Thus, EBV infection serves as a paradigm of lifelong immune control of a clinically important human tumor virus (2).

While EBV expresses more than 80 gene products during lytic, virus-producing infection, EBV-associated malignancies predominantly express only latency-associated viral proteins. These evolved to induce B cell proliferation and assist the differentiation of infected cells into the memory B cell pool, the site of long-term EBV persistence (3). All 8 latency-associated EBV antigens — 6 nuclear antigens (EBNAs) and 2 membrane proteins (LMPs) — may be found in lymphoproliferative diseases, which occur at elevated frequencies in immunocompromised individuals (e.g., after allotransplantation or in AIDS patients) (4).

EBNA3A, EBNA3B, and EBNA3C are a family of transcriptional regulators that can cooperate to regulate host genes (5–7). *EBNA3A* and *EBNA3C* are oncogenes essential for efficient transformation of B cells into lymphoblastoid cell lines (LCLs) in vitro. Together, they repress transcription of genes encoding proapoptotic BIM (*BCL2L11*) and senescence-inducing $p16^{INK4A}$ and $p14^{ARF}$ (*CDKN2A*) (8–12). Moreover, EBNA3C suppresses the ATM/CHK2-dependent DNA damage response associated with unscheduled hyperproliferation (13). In contrast, EBNA3B is dispensable for B cell transformation in vitro. The observation that EBNA3B has not been counterselected over millions of years of virus-host coevolution suggests an important role in vivo (14).

Immune control of EBV is mediated primarily by T cells. Adoptive transfer of EBV-specific T cells can eradicate virus-associated tumors (15). Furthermore, T cells specific for latency-associated EBV antigens seem to control transforming EBV infection (16). $CD4^+$ helper and $CD8^+$ cytotoxic T cells of healthy virus carriers show different preferences in their recognition of latency-associated EBV antigens. While $CD8^+$ T cells target primarily the EBNA3 and LMP2 proteins, $CD4^+$ T cells most frequently react to EBNA1 (17–20).

We generated LCLs with bacterial artificial chromosome–derived (BAC-derived) EBNA3B-deleted EBV (referred to herein as EBNA3BKO) and identified genes that differed in expression

Authorship note: Robert E. White and Patrick C. Rämer, as well as Christian Münz and Martin J. Allday, contributed equally to this work. Christian Münz and Martin J. Allday are co–senior authors.

Conflict of interest: The authors have declared that no conflict of interest exists.

Citation for this article: *J Clin Invest* doi:10.1172/JCI58092.

from wild-type EBV–infected LCLs (ref. 5 and see below). These genes included a number of cell surface markers, chemokines, and potential oncogenes, which prompted us to investigate the impact of EBNA3B deletion in vivo. To this end, we infected mice reconstituted with human immune system components (humanized NOD/SCID/$\gamma_c^{-/-}$; referred to herein as huNSG), which can recapitulate hallmarks of EBV infection and immune control in vivo (21). Even low infectious doses of EBNA3BKO virus caused highly proliferative, monomorphic B cell lymphomas that resembled diffuse large B cell lymphoma (DLBCL). The EBNA3BKO-induced tumors were devoid of T cell infiltrates, possibly because of diminished secretion of the T cell–attracting chemokine CXCL10 (also known as IP10). In line with this, CXCL10 overexpression in EBNA3BKO tumor cells led to increased T cell–mediated killing of these cells in vivo. The relevance of our findings is underlined by 2 LCLs from patients with aggressive post-transplant lymphoproliferative disease (PTLD) that have mutations in EBNA3B and display a similar phenotype to EBNA3B-deficient EBV-transformed B cells, including a decreased capacity to attract T cells. Analysis of DNA from 39 EBV-positive lymphomas identified 1 case of DLBCL that also harbored EBV encoding a truncated EBNA3B, and several other lymphomas with *EBNA3B* mutations. Thus, EBNA3B seems to behave as a tumor suppressor, attenuating the oncogenic potential of EBV and ensuring long-term survival of the persistently infected host.

Results

EBNA3BKO is more tumorigenic than wild-type EBV in mice reconstituted with human immune system components. The transcriptome of EBNA3BKO LCLs differs substantially from that of wild-type LCLs. We previously observed that more than 200 host genes exhibit altered expression levels in the absence of EBNA3B (5). To address the question of how these changes affect the in vivo biology of the virus, we used the recently established model of huNSG mice (NOD/SCID/$\gamma_c^{-/-}$ mice transplanted with human hematopoietic progenitor cells [HPCs] to reconstitute components of the human immune system; refs. 21–24). The mice used in these experiments were reconstituted with HPCs from 3 different donors. Reconstitution levels in mice 3 months after HPC injection are summarized in Figure 1A, and a detailed analysis of the reconstitution is provided in Supplemental Table 1 (supplemental material available online with this article; doi:10.1172/JCI58092DS1).

To test the consequences of *EBNA3B* deletion in vivo, we infected huNSG mice with either B95-8 wild-type EBV (referred to herein as wtBAC), EBNA3BKO, or a revertant of EBNA3BKO (referred to herein as EBNA3Brev) to control for second-site mutations. Across these experiments, we explored different infectious doses (10^3 and 10^4 Raji Green units [RGU]; ref. 25) and tested 2 independently generated EBNA3BKO preparations (Supplemental Table 1). In each experiment, groups of 5 animals were infected by i.p. injection of 10^4 RGU wtBAC, EBNA3Brev, or EBNA3BKO or were mock-infected by injection of PBS. At 4 weeks after infection, macroscopically visible tumors were present only in the spleens of animals infected with EBNA3BKO (9 of 17; Figure 1, B and C). In addition, infection with EBNA3BKO led to significant splenomegaly compared with control infection (Figure 1, B and D).

EBV-infected B cells from the spleens of all animals were identified by EBV encoded RNA-1 (EBER-1) in situ hybridization (Figure 2A); these cells also expressed CD45, CD20, HLA-DR, MUM1, CD30, BCL2, OCT2, and BOB.1, but were negative for CD15, CD10, and BCL6 (data not shown). Histological assessment showed that the spleens of wtBAC- and EBNA3Brev-infected mice exhibited polymorphic infiltrates composed of B cells of variable size, plasma cells, and histiocytes, whereas tumors from EBNA3BKO-infected spleens were monomorphic and displayed the features of a DLBCL, with fields of large EBV-infected neoplastic cells (Figure 2, B and C). The neoplasia from EBNA3BKO mice showed more proliferating cells (>90% Ki67 expression, versus 30%–60% in wtBAC and EBNA3Brev infection; Figure 2D). Moreover, EBNA3B-deficient lesions lacked substantial infiltration of T cells, in contrast to spleen sections of wtBAC- and EBNA3Brev-infected mice (Figure 2E). T cells within wtBAC- and EBNA3Brev-infected splenic lesions were greater than 70% $CD8^+$, and more than 30% expressed granzyme B (data not shown). Overall, the neoplasia in wtBAC- and EBNA3Brev-infected spleens had features akin to polymorphic PTLD (consistent with other studies of EBV infection in humanized mice; refs. 21, 24), whereas EBNA3BKO-infected spleens had the features of a non–germinal center DLBCL (non–GC-DLBCL) subtype, also known as activated B cell–like DLBCL (ABC-DLBCL).

EBNA3BKO-transformed B cells have a growth advantage in vitro and in vivo. In an in vitro transformation assay, B cells infected with EBNA3BKO proliferated earlier and faster than did cells infected with wtBAC or EBNA3Brev (Figure 3A). At 14 days after infection, we found a significant expansion of infected B cells upon infection with EBNA3BKO compared with wtBAC and EBNA3Brev (Figure 3A and Supplemental Figure 1, A and B). As these cells were expanded further, we detected more transformed B cells in cultures infected with EBNA3BKO at 28 days after initial infection (Supplemental Figure 1C). It was also noted that the EBNA3BKO LCLs had a modest survival advantage relative to wtBAC and EBNA3Brev LCLs at all time points examined when cells were cultured at high cell density (data not shown). Consistent with EBNA3BKO-infected cells having a sustained growth advantage, when we compared outgrowth of in vivo–transformed LCLs from EBV-infected huNSG mice (referred to herein as NSG-LCLs; Supplemental Table 1), we could establish those more readily from EBNA3BKO- than from wtBAC- and EBNA3Brev-infected animals (53% versus 15% and 25%, respectively; Figure 3B). Moreover, EBNA3B-deficient NSG-LCLs expanded in culture significantly faster than their wtBAC- and EBNA3Brev-transformed counterparts (Figure 3C). Finally, injection of in vitro–expanded NSG-LCLs into nonreconstituted NSG mice confirmed the more aggressive growth phenotype of EBNA3BKO NSG-LCLs in vivo, in the absence of any immune response. Transfer of these cells induced more pronounced splenomegaly (Figure 3D), and we found higher loads of cell-associated EBV DNA in the animals' spleens (Figure 3E). Therefore, loss of EBNA3B results in EBV-transformed B cells with a modest but distinct growth advantage in various contexts, both in vitro and in vivo.

EBNA3BKO cell lines derived from huNSG mice resemble in vitro–generated LCLs and cell lines with mutant EBNA3B derived from PTLD patients. We next analyzed whether, in addition to more aggressive growth, B cells transformed with EBNA3BKO in vitro and in vivo share other phenotypic characteristics. We previously observed that the expression profile of EBNA3BKO-transformed B cells differs from that of their wtBAC-transformed counterparts, and many of the differentially expressed genes encode cell surface proteins (5). We confirmed the differential expression of 6 such genes by flow cytometry. Of those tested, the integrin αL chain (*ITGAL*; also known as *CD11A*, a component of LFA-1), the inhibi-

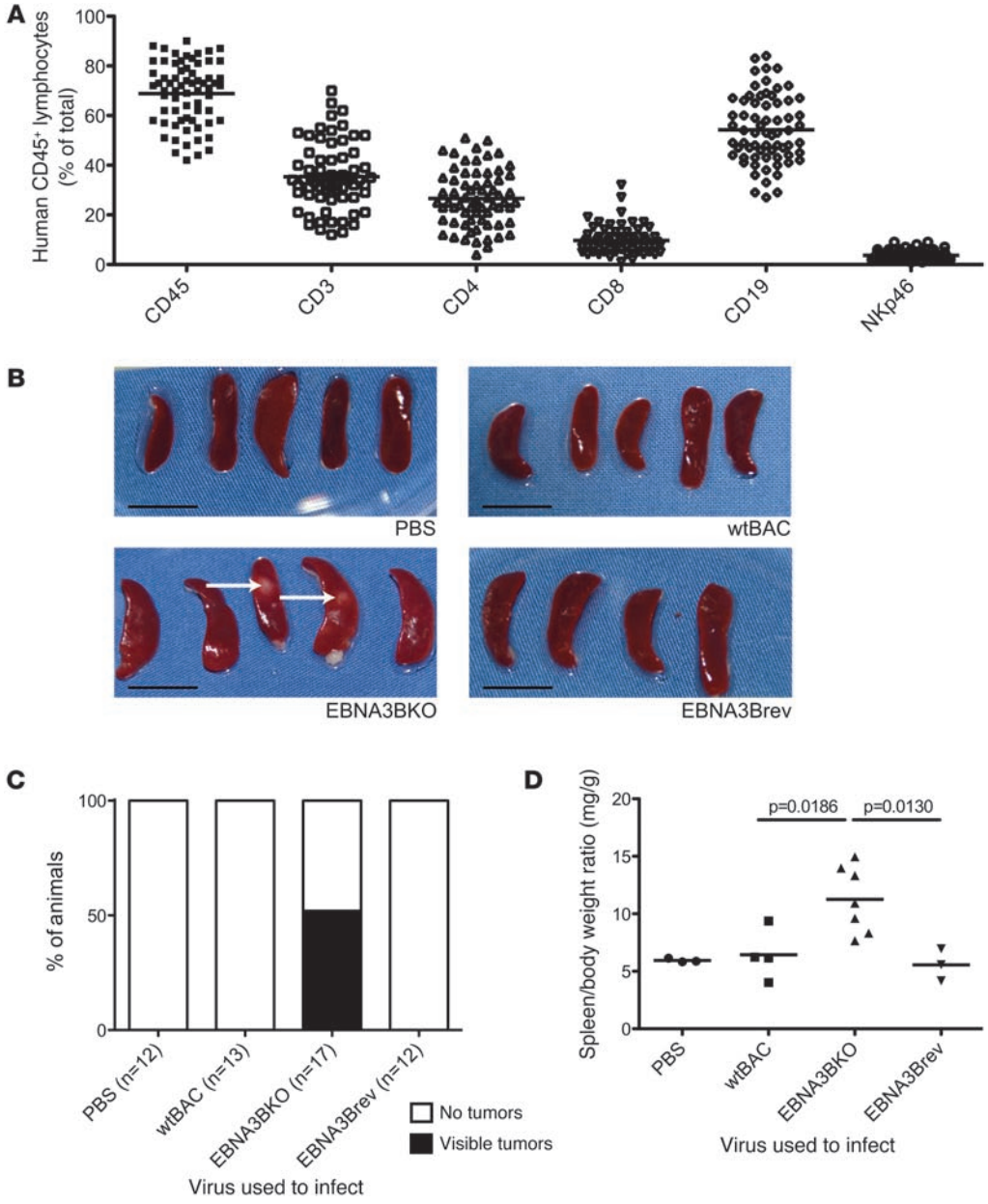

Figure 1

EBNA3BKO infection of mice with reconstituted human immune system components leads to splenomegaly and tumor formation. (**A**) Reconstitution levels of human lymphocytes in mice used to study in vivo biology of EBNA3BKO (n = 66). Frequencies of human lymphocytes in peripheral blood of mice were determined by flow cytometry. Reconstitution levels for each animal are provided in Supplemental Table 1. (**B**) Macroscopically visible tumors (arrows) in spleens of animals 28 days after infection with PBS, wtBAC, EBNA3Brev, or EBNA3BKO by i.p. injection. Scale bars: 1 cm. (**C**) Frequency of overt tumor formation 28 days after infection. (**D**) Spleen/body weight ratio 28 days after infection. Data points represent individual mice; horizontal bars represent means. Shown is 1 representative of 3 experiments (**B** and **D**) or pooled data from 3 experiments (**C**).

tory receptor *LAIR1* (also known as *CD305*), and the chemokine receptor *CXCR4* were most clearly able to distinguish EBNA3BKO from wtBAC LCLs (Supplemental Figure 2). The expression levels of these and 39 other genes found by microarray to be altered in EBNA3BKO LCLs were assessed by quantitative real-time PCR (qPCR) and confirmed to be altered (Supplemental Figure 3). Thus, loss of EBNA3B results in a substantially changed pattern of gene expression and in a distinct phenotype.

A spontaneous mutation of *EBNA3B* in a tumor of a PTLD patient has been reported previously (26). There, an initially oligoclonal lymphoma (line TRL1-pre, from patient TRL1) rapidly developed into a monoclonal tumor (line TRL1-post) that was resistant to T cell immunotherapy and proved fatal. The monoclonal tumor — diagnosed as a DLBCL (H. Heslop, unpublished observation) — as well as spontaneous LCLs (sLCLs) from peripheral blood (TRL1 LCLs) lacked full-length EBNA3B expression. This was a result of a 245-bp

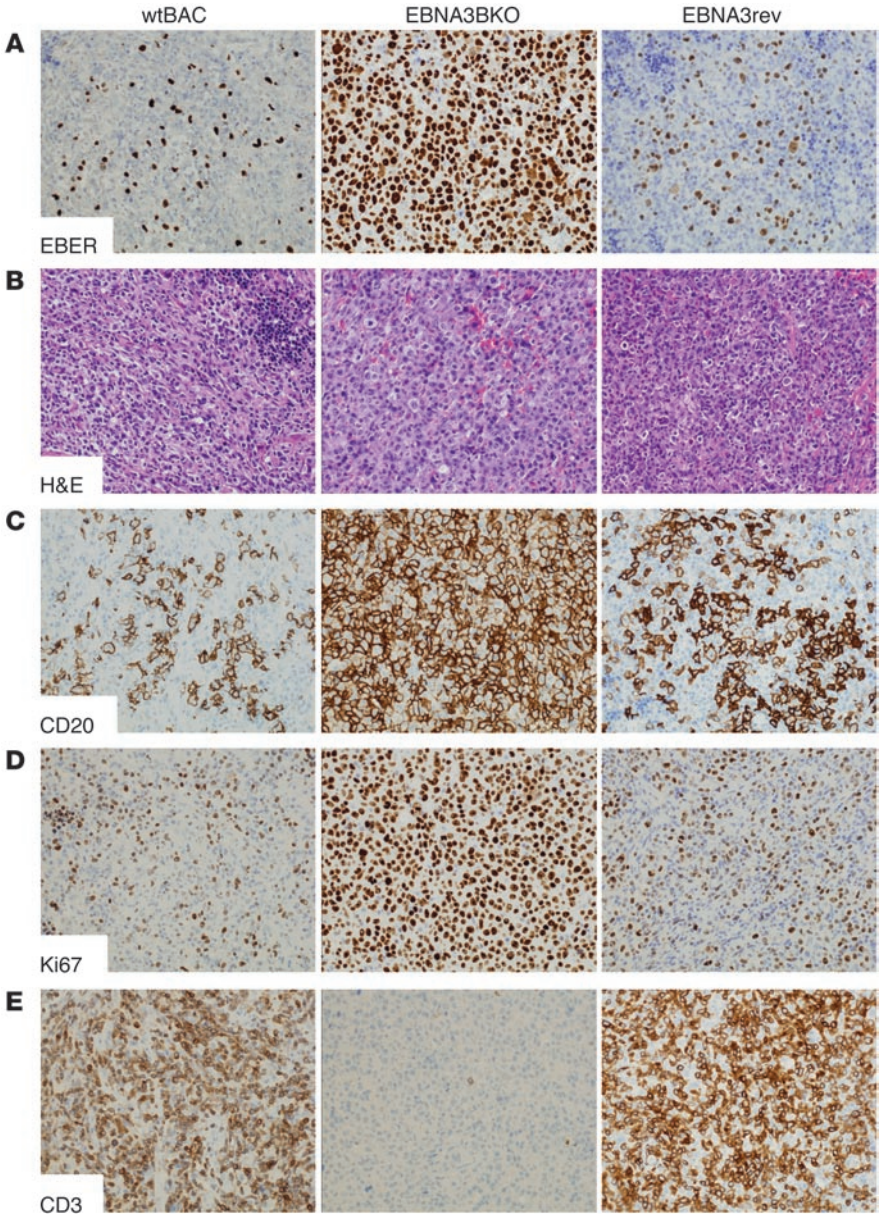

Figure 2
Histological and immunohistochemical features of splenic lesions in EBNA3BKO-, EBNA3Brev-, and wtBAC-infected mice. Shown are H&E and immunohistochemical sections from representative spleens of wtBAC- and EBNA3Brev-infected mice compared with a tumor from an EBNA3BKO-infected mouse. Original magnification, ×200. (**A**) EBER-1 in situ hybridization, showing EBV-positive cells. (**B**) H&E images showing monomorphic expansion of sheets of large lymphoid cells in the EBNA3BKO tumor — distinct from the polymorphic cellular composition of the splenic lesions (wtBAC and EBNA3Brev) — composed of a mix of lymphoid cells of varying sizes, plasma cells, and histiocytes. (**C**) Immunostaining for B cells (CD20). Nearly 100% of the cells in the EBNA3BKO-induced tumor were large B cells, whereas B cells of varying sizes represent approximately 40% of the cells in wtBAC- and EBNA3Brev-infected spleens. (**D**) Immunostaining for cell proliferation (Ki67). More than 95% of cells in the EBNA3BKO-induced tumor proliferated, versus approximately 40% in wtBAC- and EBNA3Brev-infected spleens. (**E**) Immunostaining for T cells (CD3). Only sparse infiltrating T cells were observed in the EBNA3BKO-induced tumor, whereas at least 50% of the cells in wtBAC- and EBNA3Brev-infected splenic lesions were T cells.

deletion that truncated the protein and removed the major immunodominant epitope against which the T cell immunotherapy was focused (26). Here, we report a second PTLD-derived cell line carrying a mutant EBNA3B (line TRL595). In this case, an insertion mutation resulted in a frame shift at amino acid 187 and consequent truncation of the EBNA3B open reading frame and absence of full-length EBNA3B protein (Table 1, Supplemental Data File 1, and Supplemental Figure 4). Patient TRL595 was a juvenile liver transplant recipient who developed enlarged adenoids and tonsils and an elevated EBV titer that failed to respond to modulation of immunosuppression. Histological assessment diagnosed an early PTLD with follicular hyperplasia. The patient was cured by removal of adenoids and tonsils combined with adoptive T cell immunotherapy.

Phenotypic profiling by qPCR of the tumor cells expanded in vitro from both huNSG mice and patients TRL1 and TRL595 confirmed a number of differences between the EBNA3BKO-transformed and the wtBAC- and EBNA3Brev-transformed LCLs (Figure 4A). For many genes (e.g., *CXCR7*, *CXCL10*, *IL19*, *IL10*, *IL6R*, *TNFRSF10A*, and *TNFRSF10D*), the expression levels in both patient-derived LCLs were similar to those of NSG-LCLs (Figure 4A). Cell surface expression of LAIR1 and CD11a also resembled EBNA3BKO-associated expression patterns (Figure 4B). Western blotting showed similar levels of EBV latency-associated proteins (other than EBNA3B) in mouse-derived and patient cell lines (Supplemental Figure 4).

Principal component analysis of the gene expression data for 48 genes (Supplemental Table 2) in both in vitro– and ex vivo–established LCLs (Figure 4C) separated the cell lines into 2 groups according to the virus type with which they are infected (i.e., EBNA3BKO vs. wtBAC or EBNA3Brev). Moreover, it also distinguished the source of the LCLs (i.e., in vitro or ex vivo). The PTLD-derived EBNA3B mutant cell lines clustered among the EBNA3BKO NSG-LCLs. Thus, it appears not only that deletion of EBNA3B alters the

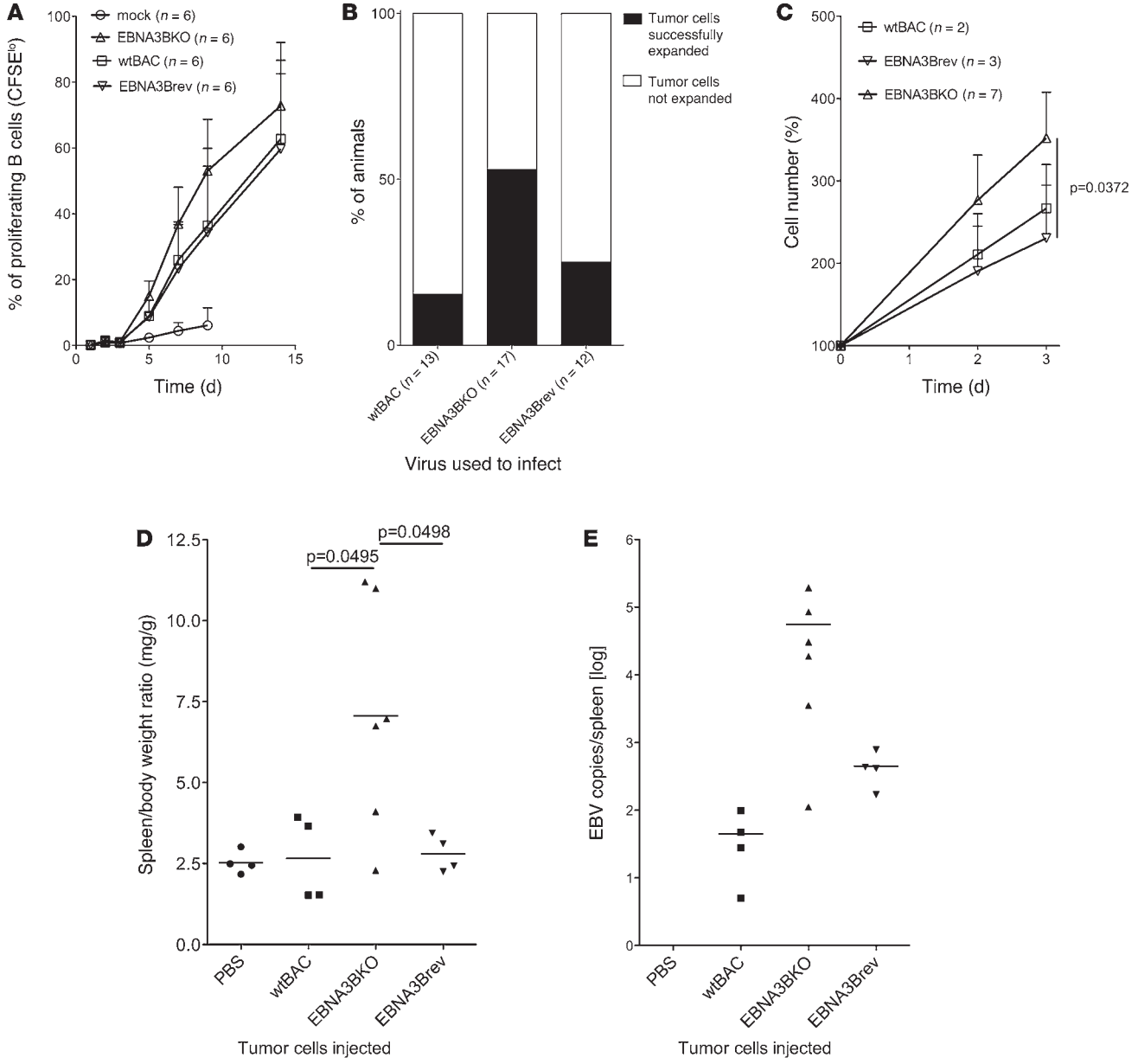

Figure 3

Transformation of B cells in vitro using EBNA3BKO is more efficient, and ex vivo–expanded tumor cells lacking EBNA3B show enhanced tumorigenicity, in unreconstituted NSG mice. (**A**) CFSE-labeled PBMCs from healthy donors were infected with EBV (2.5×10^4 RGU per 10^6 PBMCs). CFSE dilution as a surrogate of proliferation was measured over a period of 14 days. Pooled data from 6 healthy donors are shown. 2 LCLs from each of the 6 donors were assessed at the indicated time points. Data are mean ± SD. (**B**) Frequency of successful outgrowth of NSG-LCLs from spleens of animals infected with 10^4 RGU of EBV. Pooled data from 3 experiments are shown. (**C**) Growth behavior of NSG-LCLs was assessed longitudinally. 5×10^5 NSG-LCLs/ml were seeded, and cell numbers were determined at the indicated times. Data are mean ± SD. (**D**) 20 days after i.p. injection of 10^7 ex vivo–expanded tumor cells into immunodeficient NSG mice, spleens were weighed relative to total animal mass to assess splenomegaly. 1 representative of 2 experiments is shown. Statistical significance was assessed using unpaired Student's *t* test. (**E**) Splenic DNA from animals injected with EBV-transformed tumor cells was isolated 20 days after injection, and EBV DNA load was determined by qPCR. 1 representative of 2 experiments is shown. (**D** and **E**) Data points represent individual mice; horizontal bars represent means.

expression of these genes, but also that the in vivo conditioning of the cells creates a gene expression profile distinct from that of in vitro–transformed LCLs. This analysis showed that EBNA3B mutant B cell lines derived from patients resembled EBNA3BKO-transformed LCLs in huNSG mice to a remarkable extent.

B cell lymphomas contain EBNA3B mutations. In order to assess the prevalence of *EBNA3B* mutation in naturally occurring EBV-positive lymphomas, the *EBNA3B* gene was sequenced and analyzed from 190 bp upstream of its splice acceptor site to the site corresponding to amino acid 700 (of approximately 1,000). The

Table 1
Summary of potential *EBNA3B* mutations in B cell tumors

Tumor identifier	EBV type	Tumor type	Immunosuppression	Presenting location (ethnicity)	Potential *EBNA3B* mutations/unique polymorphisms[A]		
					Missense and nonsense[B]	Conservative[C]	Noncoding[D]
TRL1	1	PTLD[E]	IS	USA (European descent)	**245 bp deletion (E366-F448)**, V559F		
TRL595	1	PTLD[F]	IS	USA (Hispanic)	**G insertion at D195**		
DLBCL-3	1	DLBCL[G]	None	UK (European descent)	R8K		
ABC-1B	1	ABC-DLBCL	None	UK (European descent)			
ABC-4	1	ABC-DLBCL	IS	UK (Chinese)		–110 (TG→TA)	
ABC-D17	1	ABC-DLBCL	None	UK (NA)		G648	
ABC-DL04	1	ABC-DLBCL	None	Australia (European descent)			
ABC-H9	1	ABC-DLBCL	HIV	UK (NA)	A682P, W689C		
ABC-P8	1	ABC-DLBCL	IS	UK (NA)	P87T		
ABC-PDL10	1	ABC-DLBCL	IS	Australia (European descent)	R92H, P609R		
ABC-H31	2	ABC-DLBCL	HIV	UK (NA)			
ABC-H7	2	ABC-DLBCL	HIV	UK (NA)	**G263STOP**	G287	
ABC-DL67	1	ABC-DLBCL	None	Australia (Polynesian)	E43D, I44N, S59A, G83Y, T91S, T212P, A425T, V559L, Q575H	E64, N183, Q601	–110 (TG→CA), –35 (G→A), intron1+46(ins-T)[H]
GC-7a	1	GC-DLBCL	HIV	UK (Nigerian)			
GC-DL29	1	GC-DLBCL	None	Australia (European descent)			
GC-DL44	1	GC-DLBCL	None	Australia (European descent)			
GC-H23	1	GC-DLBCL	HIV	UK (NA)			
GC-H25	1	GC-DLBCL	HIV	UK (NA)	Q29R		
GC-PDL5	1	GC-DLBCL	IS	Australia (European descent)			
GC-H13	2	GC-DLBCL	HIV	UK (NA)			
HL01	1	HL	NA	UK (NA)			
HL02	1	HL	NA	UK (NA)	P441L		
HL03	1	HL	NA	UK (NA)			
HL04	1	HL	NA	UK (NA)	T103M		
HL05	1	HL	NA	UK (NA)			
HL06	1	HL	NA	UK (NA)			
HL07	1	HL	NA	UK (NA)		L628	
HL08	1	HL	NA	UK (NA)	PRAT441-4L (9 bp deletion)		
HL09	1	HL	NA	UK (NA)	E462K		
HL10	1	HL	NA	UK (NA)			
HL11	1	HL	NA	UK (NA)	G503S		
BL#9[I]	1	BL	NA	Uganda (NA)			
BL#27[I]	1	BL	NA	Uganda (NA)			
BL#31[I]	1	BL	NA	Uganda (NA)	Q461del (3 bp deletion)		
BL#61[I]	1	BL	NA	Uganda (NA)			
BL#63[I]	1	BL	NA	Uganda (NA)			
BL#64[I]	1	BL	NA	Uganda (NA)			
BL#74[I]	1	BL	NA	Uganda (NA)			–98A→C
BL#204[I]	1	BL	NA	Uganda (NA)			
BL#217[I]	1	BL	NA	Uganda (NA)			intron1+46(ins-T)[H]
BL#248[I]	1	BL	NA	Uganda (NA)		D359	

LCL sequence was confirmed in primary tumor material (26). Excepting the TRL595 sequence (from a tumor-derived LCL), all others are from sequencing of tumor DNA. HIV, HIV-positive patient; IS, undergoing immunosuppressive therapy to prevent transplant rejection; None, no immunosuppression; NA, information not available. [A]Analysis covered only the region of *EBNA3B* from 190 bp upstream of the start codon to amino acid 700 of the coding region. Potential mutations were defined as sequence variations that occurred in only 1 of the 41 tumor-derived or 75 LCL DNA sequences analyzed. [B]Potential mutations that changed the amino acid sequence of the protein (missense) or introduce a premature termination codon (nonsense; bold). [C]Base changes that did not alter the protein coding sequence. [D]Changes outside the amino acid coding region, expressed relative to the translational start (A of ATG is position 0) or within intron 1 (first base of the intron is position +1). [E]DLBCL. [F]Follicular hyperplasia. [G]Unclassified DLBCL subtype. [H]These 2 insertions (changing 7 consecutive T residues to 8) are the same, but are included as potential mutations as they occurred in 2 clearly distinct genetic backgrounds (Supplemental Figure 5C). [I]Described in detail previously (53).

repeat region after this point was too large to amplify reliably from formalin-fixed DNA. In all, *EBNA3B* was sequenced from 18 DLBCLs from Australia and the United Kingdom (of which 7 were GC-DLBCL, 10 were non–GC-DLBCL [i.e., ABC-DLBCL], and 1 was not classified), 11 Hodgkin lymphomas (HLs) from the United Kingdom, and 10 Burkitt lymphomas (BLs) from Uganda (Table 1 and Supplemental Data File 1). To help distinguish the natural variations in sequences from potential functional mutations, we sequenced the same region of *EBNA3B* from 44 LCLs that had been established by outgrowth from the peripheral blood of individuals from Kenya and Australia (sLCLs), some of which had been derived from individuals with underlying EBV-related disease (Supplemental Table 3 and Supplemental Data File 1). We also compared sequences with published sequences of the EBNA3B coding region from 26 Chinese sLCLs (27).

One of the non–GC-DLBCLs, sample ABC-H7, contained an EBNA3B truncation mutation (GGA to TGA substitution mutant at codon 263) and was confirmed in 3 independent PCRs (Supplemental Figure 5B). This truncation is positioned between the 2 previously described TRL mutants (Figure 5). The tumor arose in an HIV-positive individual (Table 1) infected with a type 2 EBV strain. This implies that the antioncogenic properties of EBNA3B are not restricted to type 1 virus strains.

Definitively identifying nontruncating mutations that affect EBNA3B function is challenging because of the genetic diversity of *EBNA3B*. Consistent with previous reports (27, 28), we observed little variation among the type 2 *EBNA3B* sequences, while the type 1 *EBNA3B* sequences were considerably more variable, exhibiting a number of distinct clades when arranged on a phylogenetic tree (Supplemental Figure 5C). In principle, any polymorphism that is divorced from the rest of its haplotype (i.e., a unique mutation) represents a mutation potentially associated with lymphoma development. All of these potential tumor-associated mutations are summarized in Figure 5 and Table 1.

A 60-bp in-frame deletion in the repeat region of sample ABC-D17, also found in sLCL07 (Supplemental Table 3 and Supplemental Data File 1), was a common polymorphism in the Chinese reference samples (27). Although samples ABC-DL67 and BL217 were genetically distinct (notably, ABC-DL67 is from a Polynesian individual carrying a previously described intertypic Papua New Guinea strain; refs. 29, 30), both had a single-base insertion in a run of T bases within the *EBNA3B* intron that was not seen in any other virus subtype tested. There was a 9-bp deletion in HL08, which replaced ^{441}PRAT^{444} with L. Notably, a second HL sample had a distinct potential mutation at this locus, with a unique P441L substitution. The different haplotypes before and after the HL08 deletion suggest that the deletion occurred during recombination between viruses of 2 different clades, but whether this is unique to the tumor or represents a generally circulating EBV strain cannot be deduced. An in-frame deletion was also seen in the BL sample BL#31. In this case, Q461 was deleted in a haplotype that was otherwise consistent with the major east African B95-8–like clade (Supplemental Figure 5C).

Overall, we observed that at least 1 of the 18 DLBCL biopsies tested, and perhaps as many as 9 (up to 50%), contained a mutation in *EBNA3B*, along with as many as 5 of 11 HLs and 3 of 10 BLs (up to 45% and 30%, respectively; Figure 5 and Table 1). These potential mutations appeared to predominate in the short first exon of *EBNA3B* for the DLBCLs (and was also seen in 1 HL) and around amino acids 435–465 in the BLs and HLs. Potential mutations appeared in 9 of 21 Australian sLCLs, 7 of 23 African sLCLs, and 3 of 26 Cantonese sLCLs, an overall frequency of 27%. In contrast to the tumor-derived sequences, the distribution of these possible mutations in sLCLs (which could represent the distribution of unmapped natural polymorphisms, mutations that facilitate sLCL outgrowth, or mutations associated with underlying diseases in the donors) were uncommon in the first exon (2 missense and 2 conservative unique variations), but were slightly enriched (5 of the 19 potential mutations found in sLCLs) in the small region of amino acids 435–465 (Supplemental Table 3).

Infection of mice with EBNA3BKO primes stronger systemic immune responses. We have recently shown that in vivo–primed human T cells protect huNSG mice from EBV-associated lymphomagenesis (21). Here, we observed that EBNA3BKO-induced tumors lacked infiltrating T cells (Figure 2E). Because EBNA3B gives rise to immunodominant peptides and is frequently targeted by EBV-specific T cells (16), we tested whether the absence of EBNA3B enables EBV-infected cells to escape immune recognition. Contrary to this hypothesis, however, after infection of huNSG mice with low doses of EBV (10^4 RGU), EBNA3BKO induced a significantly larger expansion of T cells in the spleen relative to wtBAC and EBNA3Brev (Figure 6A and Supplemental Figure 6). Since the majority of expanding T cells were $CD8^+$, we observed a drastic inversion of the $CD8^+$ T cell/$CD4^+$ T cell ratio compared with wtBAC or EBNA3Brev infection (Figure 6B). In addition, infection with EBNA3BKO also resulted in an increased frequency of activated HLA-DR^+ T cells (Figure 6C) and EBV-specific T cells, as indicated by higher numbers of IFN-γ–producing splenocytes in response to ex vivo restimulation with autologous LCLs (Figure 6D). Thus, EBNA3BKO infection more readily expands activated EBV-specific $CD8^+$ T cells.

EBNA3BKO-transformed B cells produce reduced amounts of the chemokine CXCL10. Despite these stronger systemic immune responses, we observed substantial tumors in animals infected with EBNA3BKO (Figures 1 and 2). However, these largely lacked T cell infiltrates (Figure 2E), which suggests that EBNA3BKO-transformed tumor cells might not express chemotactic signals to attract EBV-specific T cells. Expression profiling of LCLs and tumor-derived cell lines identified several differentially expressed chemokines and their receptors in the absence of EBNA3B (ref. 5, Figure 4A, and Supplemental Figure 3). These included the chemokine CXCL10, which is commonly expressed by EBV-induced tumors (31). CXCL10 is involved in T cell migration (32), it is induced at sites of inflammation (33), and high levels of its expression in tumor tissue are associated with prolonged disease-free survival in patients with colorectal cancer (34). *CXCL10* mRNA was expressed at low levels not only in EBNA3BKO NSG-LCLs, but also in the tumor cell lines from PTLD patients bearing *EBNA3B* mutations (Figure 7A). We detected reduced basal secretion of CXCL10 protein by EBNA3BKO NSG-LCLs and EBNA3B mutant patient LCLs during normal culture. Furthermore, these cell lines failed to upregulate CXCL10 secretion upon stimulation with IFN-γ (Figure 7B).

To test whether the reduced secretion of CXCL10 influences the migratory behavior of virus-specific T cells, we performed migration assays using previously established EBV-specific T cell clones (35, 36). Significantly fewer $CD8^+$ T cells migrated toward EBNA3BKO NSG-LCL–conditioned tumor cell supernatants (Figure 7C). This impaired attraction of T cells was partially corrected by supplementing these supernatants with CXCL10 to the level present in wtBAC-LCL– and EBNA3Brev-LCL–condi-

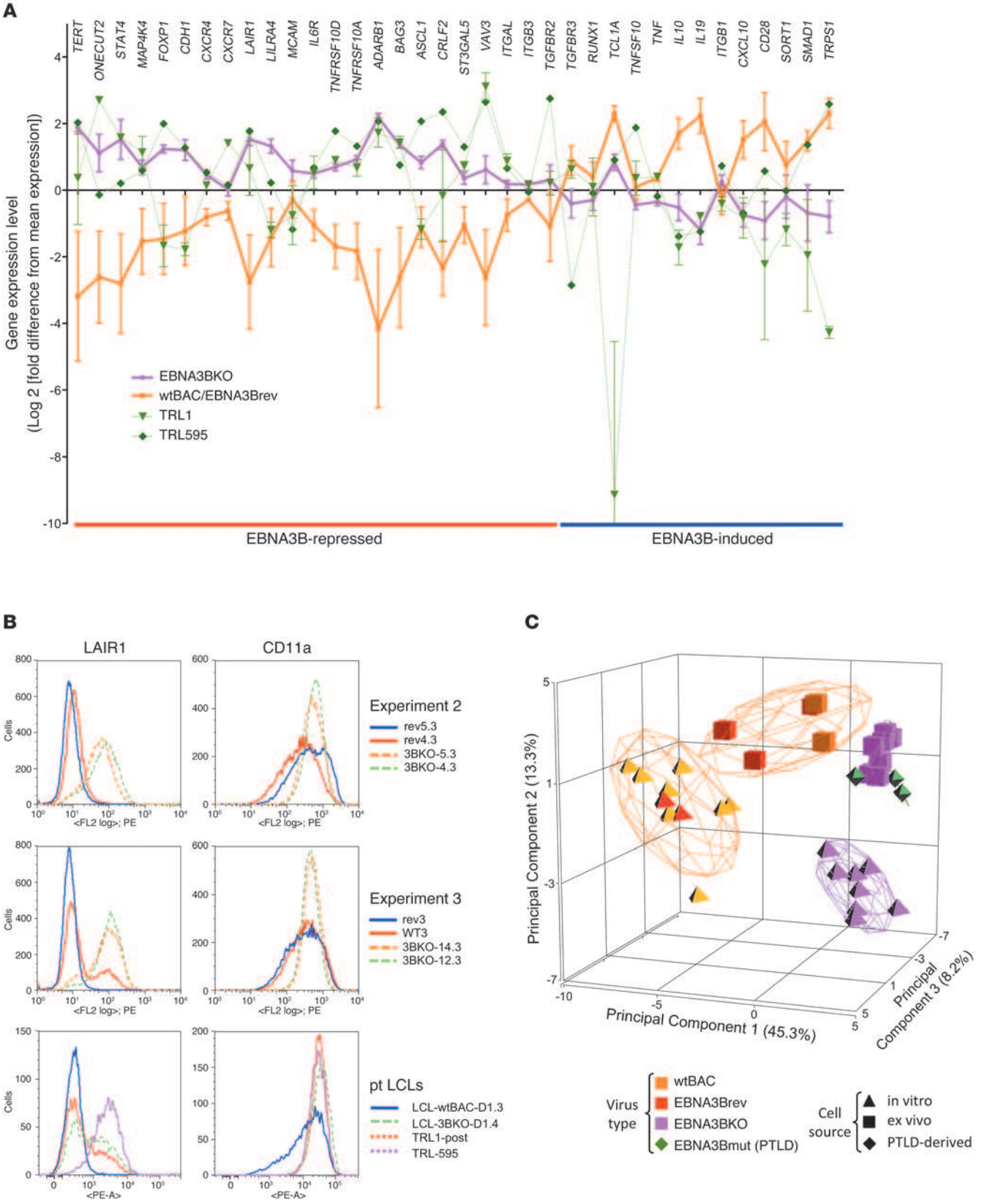
A
TERT
ONECUT2
STAT4
MAP4K4
FOXP1
CDH1
CXCR4
CXCR7
LAIR1
LILRA4
MCAM
IL6R
TNFRSF10D
TNFRSF10A
ADARB1
BAG3
ASCL1
CRLF2
ST3GAL5
VAV3
ITGAL
ITGB3
TGFBR2
TGFBR3
RUNX1
TCL1A
TNFSF10
TNF
IL10
IL19
ITGB1
CXCL10
CD28
SORT1
SMAD1
TRPS1
Gene expression level
(Log 2 [fold difference from mean expression])
EBNA3BKO
wtBAC/EBNA3Brev
TRL1
TRL595
EBNA3B-repressed
EBNA3B-induced
B
LAIR1
CD11a
Cells
<FL2 log>; PE
Experiment 2
rev5.3
rev4.3
3BKO-5.3
3BKO-4.3
Experiment 3
rev3
WT3
3BKO-14.3
3BKO-12.3
pt LCLs
LCL-wtBAC-D1.3
LCL-3BKO-D1.4
TRL1-post
TRL-595
<PE-A>
C
Principal Component 2 (13.3%)
Principal Component 1 (45.3%)
Principal Component 3 (8.2%)
Virus type
wtBAC
EBNA3Brev
EBNA3BKO
EBNA3Bmut (PTLD)
Cell source
in vitro
ex vivo
PTLD-derived

Figure 4
PTLD-derived LCLs lacking EBNA3B phenotypically resemble those derived from infected mice. (**A**) Relative gene expression levels, measured by qPCR using Taqman low-density arrays, normalized against 4 endogenous controls, and plotted on a $\log_2$ scale as the distance from the geometric mean expression for that gene across all cell lines. Data are mean ± SEM for the EBNA3BKO and combined wtBAC and EBNA3Brev cell lines. Also shown are expression levels in the patient-derived cell lines, for which error bars indicate expression values of the 2 TRL1 lines. Data points are connected to clarify data trends. (**B**) Flow cytometry profiles for LAIR1 and CD11a expression in ex vivo–expanded cells from 2 mouse experiments and EBNA3B mutant PTLD patients (ptLCLs). Each plot contains the same number of gated events to facilitate comparison of samples within the same experiment. (**C**) Principal component correlation analysis of cell lines based on gene expression data from qPCR analysis of the 48 genes shown in Supplemental Figure 3. Samples are identified by the infecting virus (color) and whether the LCLs were established in vitro or ex vivo (shape). Groups by virus and LCL type are indicated by overlaid icosahedrons colored by virus type; wtBAC and EBNA3Brev were considered as a single group, and TRL1 and TRL595 lines were separated. Percent contribution of each principal component to total variation is indicated on the respective axis.

tioned supernatants. Because similar impairment of migration was detected for EBV-specific $CD4^+$ T cells (Supplemental Figure 7), we tested whether the observed reduction in expression and secretion of CXCL10 in EBNA3BKO-transformed tumor cells protected the cells from T cell–mediated killing, both in vitro and in vivo. For these assays, we transduced EBNA3BKO LCLs with lentiviruses capable of constitutively expressing CXCL10 (referred to herein as EBNA3BKO-LV[CXCL10]-LCLs). In the absence of IFN induction, these cells secreted CXCL10 levels similar to those of wtBAC- and EBNA3Brev-transformed LCLs, and considerably more than those of nontransduced and control vector–transduced EBNA3BKO LCLs (EBNA3BKO-LV[ctr]-LCLs; Supplemental Figure 8A). IFN induction of CXCL10 remained partially impaired in the EBNA3BKO-LV[CXCL10]-LCLs. In in vitro killing assays, nontransduced as well as transduced EBNA3BKO LCLs were as susceptible to lysis mediated by an autologous polyclonal T cell line as their wtBAC and EBNA3Brev counterparts (Supplemental Figure 8, B and C). In vivo, however, EBNA3BKO-LV[CXCL10]-LCLs were preferentially depleted in the presence of autologous, polyclonal EBV-specific T cell lines compared with EBNA3BKO-LV[ctr]-LCLs (Figure 7, D and E). Taken together, these data suggest that EBNA3BKO-transformed B cells are less able to attract both $CD4^+$ and $CD8^+$ T cells to the tumor microenvironment, that this reduced T cell attraction protects the EBNA3BKO LCLs from T cell–mediated killing, and that this is at least partially due to the reduced expression of CXCL10 by EBNA3BKO LCLs.

Discussion

Using a humanized mouse model for EBV infection and disease, we have shown that the loss of a single EBV latency-associated gene product, EBNA3B, caused a profound change in the character, immune evasion, and aggressiveness of EBV-associated cancer. EBNA3B was responsible for substantial changes in the expression of host genes, and these changes altered cell surface markers, chemokine expression, and growth behavior of mutant virus–transformed B cells. This became manifest as a striking phenotype in vivo: the development of monomorphic DLBCL-like tumor masses that disrupted splenic architecture and lacked infiltrating T lymphocytes. Our discovery of EBV with mutant *EBNA3B* in human lymphomas emphasized the predictive power of this humanized mouse model.

Escape from HLA-A11–restricted recognition of EBNA3B was previously suggested as the cause of the uncontrolled growth of a post-transplant DLBCL in patient TRL1 (26), whose cells were used in the present study. However, the newly described patient TRL595 was HLA-A11 negative, and none of the HPC transplants used to reconstitute the mice in our study expressed the respective restriction elements for immunodominant EBNA3B epitopes, including HLA-A11 (Supplemental Table 1). Furthermore, in contrast to diminished EBV-specific immune control in the absence of EBNA3B in patient TRL1, huNSG mice infected with the EBNA3BKO virus displayed significantly greater T cell expansion than did wtBAC- or EBNA3Brev-infected controls. These expanded T cells recognized in vivo–transformed wild-type and mutant tumor cells at higher frequencies than did T cells from wild-type and uninfected controls. Thus, infection with EBNA3BKO appears to prime EBV-specific T cell responses more efficiently. This is likely due to the elevated antigenic load provided by more robustly proliferating B cells transformed by the mutant virus. These antigens can be used for systemic T cell priming by dendritic cells (37).

Despite this efficient systemic T cell priming, however, we showed that the chemoattraction of T cells to EBNA3BKO-transformed B cells was reduced in vitro and that EBNA3B-negative tumors displayed no significant T cell infiltration in vivo. This is probably, at least in part, because EBNA3BKO-transformed tumor cells secreted reduced amounts of the chemokine CXCL10. The regulation of CXCL10 by EBV is not simply a matter of its upregulation by EBNA3B and IFN; it is complex and finely balanced. As summarized in Supplemental Figure 9, recent studies have shown that, in the context of EBV infection in LCLs, EBNA3A can repress *CXCL10* expression (5, 6). We showed that while basal *CXCL10* expression and secretion was low, it required EBNA3B to retain its inducibility by IFN (Figure 7B). This suggests that EBNA3B potentiates the expression of CXCL10 and counteracts its repression by *EBNA3A* and perhaps by other EBV genes.

Recent reports indicate an important role of CXCL10 in tumor immune control (34). Cytotoxic T lymphocytes (CTLs) used for the treatment of EBV-related lymphoproliferative disease consistently express CXCR3, the receptor for CXCL10 (38). In line with these findings, we observed increased lysis of EBNA3BKO LCLs ectopically expressing CXCL10 by autologous T cells in vivo. These findings suggest that the silencing of CXCL10 in EBNA3B mutant cells allows developing tumors to escape immune control by infiltrating EBV-specific T cells, thereby enabling them to establish stable and substantial tumor masses.

Infection of huNSG mice with EBV induces a polymorphic lymphoproliferation that becomes full-blown lymphoproliferative disease in the absence of T cell surveillance (21). Here, we observed a similar polymorphic phenotype in wtBAC- and EBNA3Brev-infected animals, but EBNA3BKO induced monomorphic lymphomas, increased splenomegaly, and gross tumor formation in greater than 50% of animals. Furthermore, EBNA3BKO cell lines were more frequently established from splenocytes and appeared to proliferate faster than their wtBAC and EBNA3Brev counter-

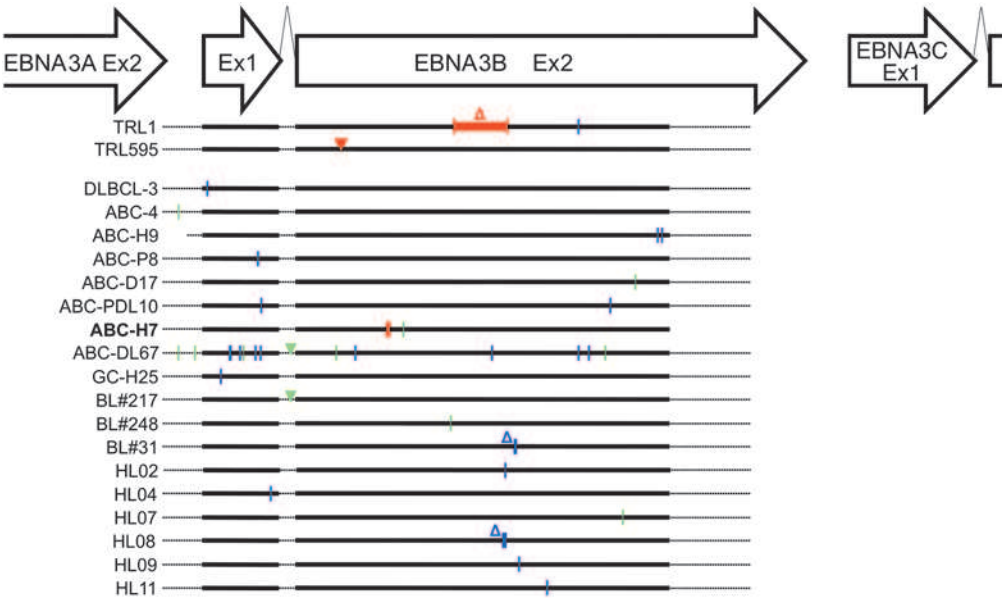

Figure 5

EBNA3B mutations identified in lymphomas. Schematic representation (to scale) of the *EBNA3B* gene locus (flanked by *EBNA3A* and *EBNA3C* as indicated) and, below, visual representation of definite and potential *EBNA3B* mutations (i.e., tumor-only polymorphisms) identified by comparing 39 lymphoma samples with 69 sLCLs. Only those samples with at least 1 possible mutation are shown. Bold horizontal lines indicate the coding region analyzed for mutations (amino acids 1–700). Dashed horizontal lines indicate the extent of sequence used in the sequence alignment (see Supplemental Data File 1). *EBNA3B* mutations identified in LCLs grown from PTLD tumors (i.e., TRL1 and TRL595) are shown for comparison. Red symbols, mutations leading to a premature STOP codon; blue symbols, potential missense mutations; green symbols, DNA changes that do not alter protein sequence. Vertical lines represent substitution mutants/polymorphisms; inverted triangles indicate insertional mutations; and deletion mutants are shown by open triangles, with the associated box indicating the deletion size. Sample ABC-H7 (bold) contains a truncation mutation (GGA to TGA substitution mutant at codon 263) positioned between the 2 previously described TRL mutants. See Table 1 for details of these mutations and characteristics of all tumors analyzed.

parts in vitro and upon transfer into immunocompromised mice. This emphasizes that the EBNA3BKO tumors differ fundamentally from wild-type EBV–driven B cell lymphoproliferations in their morphology, aggressiveness, and capacity to escape immune recognition. No one of the described components — B cell transformation process, LCL proliferation, and immune escape — can solely explain the drastic differences we observed between wtBAC or EBNA3Brev infection and EBNA3BKO infection. Our data suggest that a combination of at least these 3 components leads to this striking phenotype. The monomorphic phenotype of the EBNA3BKO tumors might result from a defect in terminal differentiation that could also be linked to the EBNA3B deficit.

Validating the clinical relevance of the huNSG model, the solid ABC-DLBCL–like tumors in EBNA3BKO-infected mice were reminiscent of the post-transplant DLBCL that extensively infiltrated the lungs of patient TRL1 at autopsy (26). Moreover, the similarities in gene expression profiles of the patient- and huNSG mouse–derived LCLs are considerable. Of particular note, CXCL10 expression was reduced in both PTLD-derived lines, and might therefore have contributed to the failure of CTL immunotherapy in patient TRL1. An initial survey of *EBNA3B* status in a set of human tumor samples showed that 1 of 10 ABC-DLBCLs carried a truncation mutation in the first 2 kb of *EBNA3B*, similar to those found in the cases of PTLD. Moreover, 6 of the 9 other ABC-DLBCLs (as well as the 1 unclassified DLBCL) were found to contain potential tumor-associated mutations in *EBNA3B*. In contrast, only 1 in 7 GC-DLBCLs had a potential mutation (Figure 5 and Table 1). It is perhaps significant that the 2 EBNA3B-deficient PTLDs and the ABC-DLBCL had an activated B cell phenotype, consistent with the growth program of EBV latency-associated gene expression that is found in LCLs and that normally includes expression of the EBNA3 proteins. However, 5 of 11 HLs and 3 of 10 BLs were found to carry potential EBNA3B mutations (Figure 5); these potential mutations were clustered within the first exon and among amino acids 435–465 (for HL/BL) and included 1 HL and 1 BL with in-frame deletions not seen in any other reported *EBNA3B* sequence. Neither of these regions contains any known CTL epitopes (16). Mutations in *EBNA3B* could disrupt the protein's interaction with binding partners, affect the splicing of the internal intron, or compromise the poorly understood alternative splicing process through which the EBNA3s and EBNA1 are joined for their translation (39). However, because no functional domains to our knowledge have been definitively identified in the protein, the functional relevance of specific mutations cannot be predicted.

From this initial study, it is not possible to deduce the extent to which disrupting EBNA3B function contributes to lymphomagenesis. We were able to analyze the first 700 amino acids of *EBNA3B* and found mutations in 1 of the 3 type 2 EBVs analyzed. This suggests that EBNA3B's apparent function as a tumor suppressor applies across all EBV strains and is not an

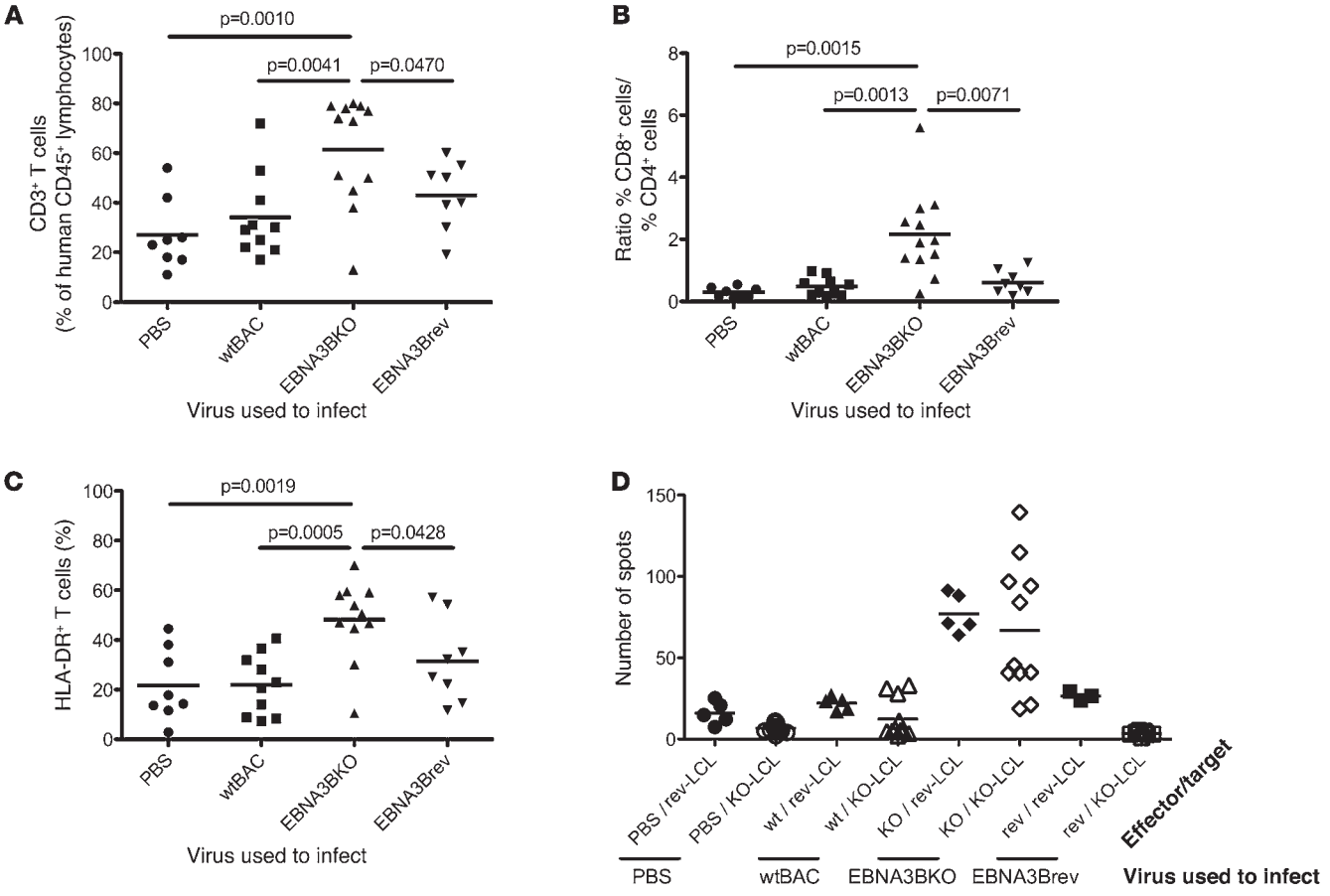

Figure 6

Infection with EBNA3BKO primes stronger immune responses than infection with wtBAC or EBNA3Brev. Splenocytes from control or EBV-infected animals were isolated 28 days after infection. (**A**) CD3+ T cell frequency among human CD45+ lymphocytes, determined by flow cytometry. (**B**) Ratio of CD8+ T cell to CD4+ T cell frequency. (**C**) Activation of T cells, assessed by HLA-DR expression on their surface. (**D**) Isolated splenocytes were depleted of human B cells and cocultured with ex vivo–expanded tumor cell lines to measure EBV-specific IFN-γ secretion, determined using ELISPOT assays and expressed as the number of IFN-γ–specific spots per 2×10^5 cells. Pooled data from 2 experiments are shown. (**A**–**D**) Data points represent individual mice; horizontal bars represent means.

idiosyncrasy of the type 1 B95-8 strain. The degree of polymorphism in type 1 EBVs makes identifying functional mutants in type 1 EBV difficult. This phenomenon has been previously reported in the *EBNA2* and *EBNA3* genes (27, 28, 40). We suggest that major epidemiological and functional analyses will be required to assess the natural range of EBV variation and, more importantly, to identify tumor-associated mutations.

Our identification of independent *EBNA3B* mutations in 2 cases of DLBCL (both HIV and PTLD associated) and in an early PTLD lesion, as well as likely mutations in HL and BL, suggests that loss of EBNA3B function might be a frequent contributor to the evolution of various types of aggressive lymphoma. The possibility that *EBNA3B* is mutated (and, by implication, would otherwise be functional) in a wide range of lymphomas cannot be excluded. *EBNA3* gene expression in primary tumors is poorly understood — although it is known that some BLs and DLBCLs can express EBNA3s (29, 41), there is no evidence for conventional EBNA3 transcripts in most BLs or HLs (42). An oncogenic role for an EBNA3B mutant EBV in initiating tumorigenesis in progenitors of these lymphomas is an intriguing possibility.

There has long been a suspicion that EBV mutation may play a role in EBV-related cancers. The only previously reported example of lymphoma-associated mutation in EBV is the subset of EBNA3-expressing BLs that have undergone deletion of EBNA2 and part of EBNA-LP (41). The identification herein of a second tumor-associated type of mutation in EBV suggests a broader paradigm, in which EBV mutation or the mutational imbalance of expression between viral oncogenes and tumor suppressors plays a role in EBV-associated tumorigenesis.

While it is well established that EBV encodes oncogenes, we believe EBNA3B represents the first example of a viral gene whose absence can increase the oncogenic potential of the virus; thus, it may represent a novel class of virus-encoded tumor suppressors. Our data suggest that EBNA3B is a tumor suppressor that normally restrains proliferation of EBV-transformed B cells and allows them to attract T lymphocytes via chemokine secretion. This might help to maintain chronic viral infection without severe morbidity and mortality from lymphoproliferative disease, representing an evolutionary adaptation to minimize oncogenic risk to the host.

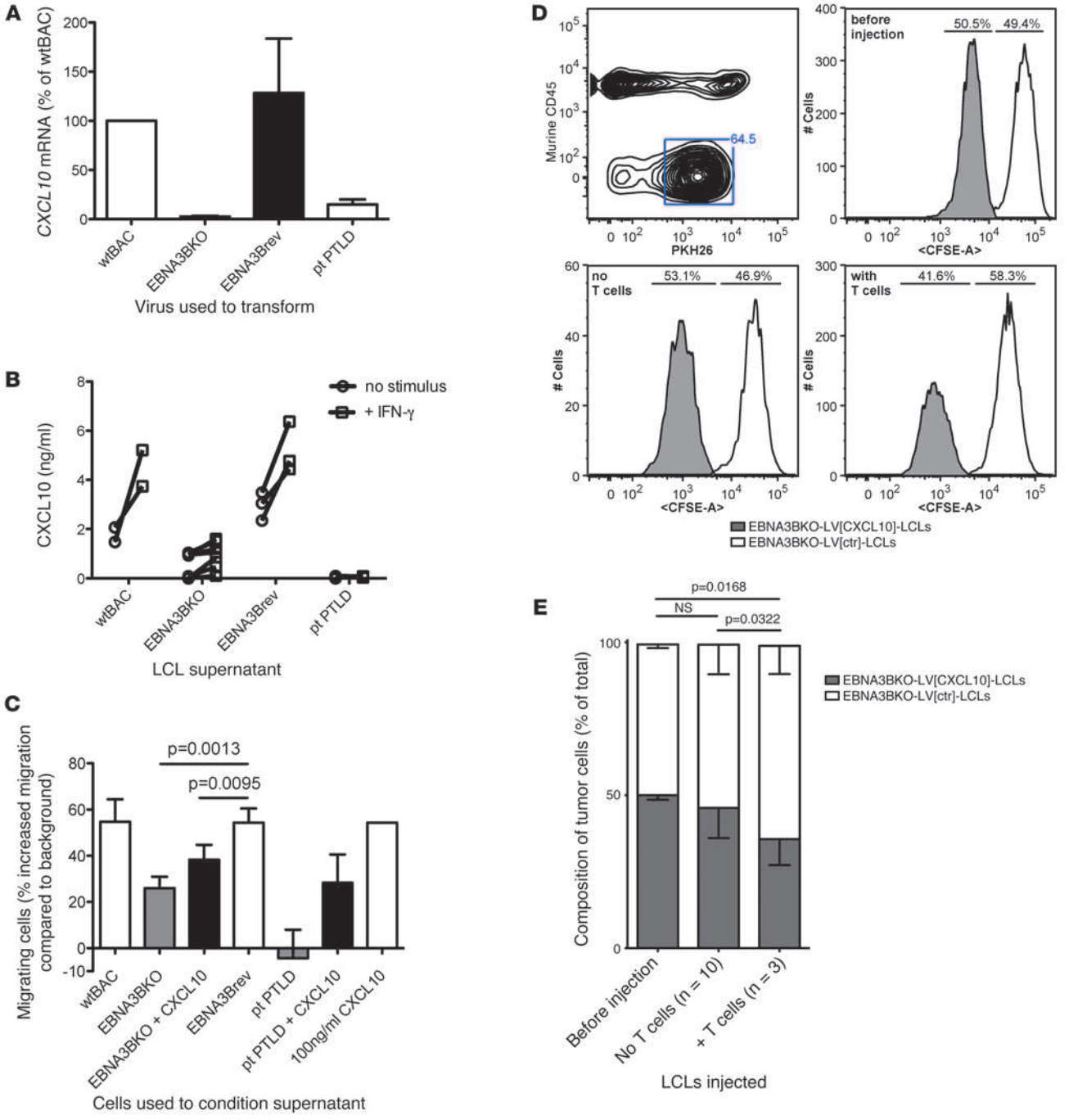

Figure 7

EBNA3BKO-transformed tumor cells produce and secrete reduced amounts of CXCL10 and attract fewer EBV-specific T cells. (**A**) *CXCL10* mRNA levels, determined by qPCR, normalized to *GAPDH* expression, and expressed relative to *CXCL10* expression of wtBAC-transformed tumor cells. (**B**) CXCL10 protein levels, determined in culture supernatants of EBV-transformed tumor cells by ELISA after 24 hours of culture with or without added IFN-γ. (**C**) Migration of the EBV-specific $CD8^+$ T cell clone MS.B11 toward tumor cell–conditioned supernatants, assessed by Transwell migration assay. For EBNA3BKO-transformed tumor lines and patient PTLD LCLs, CXCL10 was supplemented as indicated to reach concentrations present in wtBAC- and EBNA3Brev-conditioned supernatants. (**A**–**C**) Shown is 1 representative of 2 experiments with 2 wtBAC, 3 EBNA3Brev, 7 EBNA3BKO, and 2 patient PTLD LCLs (TRL1-post and TRL595). (**D** and **E**) Killing of CXCL10-reexpressing EBNA3BKO LCLs by an autologous T cells line was tested in vivo. LCLs were transduced with a CXCL10-expressing lentivirus or control virus. In vivo killing assays were performed after labeling of LCLs with PKH26 and high or low concentration of CFSE. (**D**) Example of FACS gating for the experiment, and representative histograms for tumor cell composition before and after injection in the presence or absence of autologous T cells. Percentages denote $CXCL10^+$ and $CXCL10^-$ cells as a fraction of total tumor cells. (**E**) Summary of 3 experiments performed as described in **D**. (**A**–**E**) Data are mean ± SD.

Methods

Recombinant EBV and LCLs. Generation of EBNA3BKO and EBNA3Brev is described elsewhere (8). Generation and microarray analysis of in vitro–transformed EBNA3BKO and wtBAC LCLs are also previously published (5). EBNA3Brev LCLs in D2 and D3 genetic backgrounds were generated alongside those described previously. The same virus preparations used to generate all of these LCLs were also used for the in vivo infections described herein. Additional in vitro–transformed LCLs from a fourth donor (D4; included in the qPCR analysis) were made using different virus preparations, by infection of peripheral blood cells isolated by Ficoll gradients from buffy coat residues. For infection of huNSG mice, animals were injected i.p. with 100 μl of virus concentrated from filtered culture supernatants by ultracentrifugation and resuspended in PBS (or with 100 μl PBS alone).

To generate NSG-LCLs ex vivo, human B cells were isolated from spleen suspensions using CD19 microbeads (Miltenyi Biotec). Isolated B cells were plated into 96-well U-bottom plates (5×10^5 cells/well) and cultured in RPMI 1640 supplemented with 10% FCS. Outgrowing cells were further expanded by seeding at 3×10^5 cells/ml and splitting at $6–8 \times 10^5$ cells/ml.

Generation of a polyclonal EBV-specific T cell line. An EBV-specific T cell line was generated as previously described (43). In brief, PBMCs isolated from peripheral blood of a healthy donor (HLA-A*0201, HLA-A*6801, HLA-B*4402, HLA-B*0702, HLA-C*0501, HLA-C*0702, HLA-DRB1*1501, HLA-DRB1*0401) were stimulated with autologous, irradiated EBNA3BKO LCLs at a PBMC/LCL ratio of 1:40. After 7 days, cells were restimulated with irradiated LCLs (1:4 PBMC/LCL ratio), and after 3 additional days, the medium was supplemented with a low dose of IL-2 (25 IU/ml; NIH cytokine repository). Cultures were subsequently supplemented with 25 IU/ml IL-2 2 times per week and stimulated with autologous, irradiated EBNA3BKO LCLs (1:4 PBMC/LCL ratio) every 7 days.

Lentiviral transduction of LCLs. A lentiviral expression vector encoding CXCL10 (pLenti-CMV-CXCL10-Puro) was generated by cloning of cDNA corresponding to CXCL10 (IMAGE Id 4274617; Source BioScience) into pENTR1A (44) (Addgene plasmid 17398). Gateway LR clonase (Invitrogen) was thereafter used to clone the insert into pLenti-CMV-Puro-DEST (44) (Addgene plasmid 17452). Using the resulting vector, lentiviral particles were generated as described elsewhere (45). LCLs autologous to the polyclonal T cell line described above were transduced with the lentiviral particles, and successfully transduced cells were selected in the presence of Puromycin (700 ng/ml; Invivogen) for 14 days. As a control, LCLs were transduced with pLenti-CMV-Puro-DEST.

Monitoring of B cell transformation by CFSE dilution and growth kinetics. The capacity of wtBAC, EBNA3BKO, and EBNA3Brev to transform B cells into LCLs was analyzed using a flow cytometry–based proliferation assay. PBMCs were isolated from healthy donor buffy coat residues (Blutspendedienst Zürich). Initial frequency of B cells was determined using flow cytometry, and cells were labeled with CFSE (Sigma-Aldrich). 10^6 CFSE-stained cells were thereafter seeded into 96-well flat-bottom plates and infected with EBV by addition of 2.5×10^4 RGU EBV per well. Cyclosporin A (Sigma-Aldrich) was added to a final concentration of 1 μg/ml. CFSE dilution as a surrogate marker of proliferation was monitored by flow cytometry 1, 2, 3, 5, 7, 9, and 14 days after infection. CFSE fluorescence on day 1 was set as a cutoff value, and viable B cells with less fluorescence at a given time point were considered to have proliferated. Absolute number of live B cells per well was determined 14 days after infection. Cells were thereafter expanded, and the total number of outgrowing B cells was calculated from recounting at 28 days after infection.

Generation of mice with reconstituted human immune system components and infection with EBV. NSG mice (NOD/LtSz-scid IL2Rγnull) were obtained from the Jackson Laboratory and raised under specific pathogen–free conditions. Mice were reconstituted with human HPCs as described previously (21, 46, 47). In brief, human fetal liver tissue (obtained from Advanced Bioscience Resources) was minced and treated with 2 mg/ml collagenase D (Roche). $CD34^+$ HPCs were isolated from the resulting cell suspension using the direct $CD34^+$ Progenitor Cell Isolation Kit (Miltenyi Biotec). 2- to 5-day-old NSG mice were irradiated with 1 Gy and injected intrahepatically with $1–2 \times 10^5$ $CD34^+$ HPCs 6 hours after irradiation. Reconstitution with human immune cells in peripheral blood was analyzed 12 weeks after HPC transfer by flow cytometry. Upon confirmation of reconstitution, huNSG mice were infected with EBV by i.p. injection.

Histology, immunohistochemistry, and RNA in situ hybridization. Splenic tissue was sliced and fixed in 10% buffered formal saline for 18–24 hours and processed paraffin embedding. 4-μm-thick sections were cut and stained with H&E and for a panel of immunostains. Immunohistochemistry was performed using mouse anti-human monoclonal antibodies and standard immunohistochemical procedures on BOND-MAX automated immunohistochemistry system (Leica Microsystems). Appropriate positive and negative controls were included. For in situ hybridization, appropriate care was taken to preserve the RNA, and EBER-1 probe was used on a BOND-MAX automated system. A control probe to evaluate RNA preservation was used, and an EBV-positive classical HL sample served as an external positive control.

Analysis of T cell dynamics upon EBV infection. 4 weeks after infection, mice were sacrificed, and single-cell suspensions were generated from their spleens. The composition of the human lymphocyte compartment within these organs was analyzed by flow cytometry.

Analysis of EBV-specific T cell responses. $CD19^-$ splenocytes were cryopreserved in liquid nitrogen and later analyzed for EBV-specific T cell responses after stimulation with isolated, EBV-positive tumor cells by using an IFN-γ–specific ELISPOT assay (BD Bisosystems) as described previously (21). In brief, CD19-depleted splenocytes were cocultured with autologous ex vivo–expanded tumor cells at a ratio of 1:4 for 18 hours. IFN-γ spots were counted using an ELISPOT reader (ELR02; Autoimmun Diagnostica).

Transfer of ex vivo–expanded tumor cells into NSG mice. In vivo growth behavior of in vitro–expanded tumor cells was analyzed by i.p. injection of 10^7 NSG-LCLs, resuspended in 100 μl PBS, into 6- to 8-week-old unreconstituted NSG mice (48). After 20 days, spleen size and splenic EBV DNA load was assessed. To quantify splenic EBV DNA loads, splenocytes were isolated and counted, and DNA was isolated from $2–5 \times 10^6$ splenocytes. EBV DNA load within this portion was analyzed, and total DNA present in the spleen was back-calculated.

CXCL10 ELISA and T cell migration assays. CXCL10 content in culture supernatants of EBV-transformed tumor cells was measured using a CXCL10-specific ELISA (Peprotech) according to the manufacturer's instructions. For that, 10^6 tumor cells/ml medium were cultivated for 24 hours with or without the addition of IFN-γ at 250 IU/ml. Supernatants were filtered using 0.45-μm filters. For T cell migration assays, the EBV-specific T cell clones BC-E122 ($CD4^+$, HLA-DR7 restricted, recognizing $EBNA1_{551–570}$; ref. 36) and MS-B11 ($CD8^+$, HLA-B8, $EBNA3A_{325–333}$; ref. 49) were expanded and cultured as previously described (19). Supernatants from wtBAC-, EBNA3Brev-, and EBNA3BKO-transformed NSG-LCLs were collected after 24 hours of stimulation with IFN-γ (250 IU/ml; Peprotech). 10^6 EBV-specific T cells were added to the upper chamber, and 600 μl tumor cell supernatant to the lower chamber, of a 3-μm Transwell insert (24 well; BD Falcon), and T cell migration toward tumor cell supernatant was measured after 24 hours. When indicated, EBNA3BKO-conditioned supernatants were supplemented with recombinant human CXCL10 (Peprotech) to levels present in wtBAC- and EBNA3Brev-conditioned supernatants.

In vitro killing assay. In vitro killing assays were performed as previously described (50), with minor modifications. Target cells (LCLs) were stained

with CFSE (1 μM) and cocultured with effector cells (autologous EBV-specific T cells) at different effector/target ratios for 6 hours, after which cells were harvested. TO-PRO-3 (Sigma-Aldrich), a membrane-impermeable DNA stain, was added to each culture (1 μM final concentration), and cells were analyzed by flow cytometry. Background and maximum TO-PRO-3 staining were obtained by incubation of target cells with medium and detergent (Saponin; Sigma-Aldrich), respectively. Specific lysis was calculated as (% TO-PRO-3$^+$CFSE$^+$ cells in T cell–LCL coculture − % TO-PRO-3$^+$CFSE$^+$ cells in medium)/(% TO-PRO-3$^+$CFSE$^+$ cells in detergent − % TO-PRO-3$^+$CFSE$^+$ cells in medium) and expressed as a percentage. T cell line autoreactivity was tested using PHA-transformed (Sigma-Aldrich) autologous T cell blasts (51). As an HLA-mismatched control, LCL 721.45 was used (52).

In vivo killing assay. For in vivo killing assays, EBNA3BKO-LV[CXCL10]-LCLs and EBNA3BKO-LV[ctr]-LCLs (transduced with pLenti-CMV-CXCL10-Puro and control vector, respectively) were labeled with PKH26 (Sigma-Aldrich) and with different concentrations of CFSE (CFSE^{lo},1 μM; CFSE^{hi}, 10 μM). 1×10^7 LCLs of each of the 2 lines were injected i.p. into nonreconstituted NSG mice followed by i.p. injection of 2×10^6 autologous EBV-specific T cells (1:10 effector/target ratio). 4 hours after injection, mice were euthanized, and a peritoneal lavage was performed. The composition of the peritoneal cells was assessed by flow cytometry. To avoid a bias by the differential CFSE staining, in 2 of 3 experiments, EBNA3BKO-LV[CXCL10]-LCLs were labeled CFSE^{lo}, whereas in 1 of 3 experiments, EBNA3BKO-LV[ctr]-LCLs were labeled CFSE^{lo}.

Flow cytometry and Western blotting. Human cell surface markers were analyzed using the following monoclonal antibodies: Pacific Blue–conjugated anti-CD45 (clone HI30), FITC- or PE- conjugated anti-CD3 (HIT3a), APC-Cy7–conjugated anti-CD4 (RPA-T4), PE- or Alexa Fluor 700–conjugated anti-CD8 (RPA-T8), PE-Cy7–conjugated anti-CD19 (HIB19), Alexa Fluor 488–conjugated anti-CD45RO (UCHL1), all from Biolegend; APC-conjugated anti-NKp46 (9E2) from BD Biosciences — Pharmingen; anti-CD11a (HI111), anti-CD61 (VI-PL2), anti-DR4 (TNFRSF10A – clone DJR1), and APC-conjugated anti-CXCR4 (12G5), all from eBiosience; and PE-conjugated anti-LAIR1 (342219) and anti-MCAM (128018), both from R&D Systems. Flow cytometry was performed using a CyanADP (Beckman Coulter) and a FACS-Canto II or LSRII Fortessa flow cytometer (both from BD Biosystems). Data analysis was performed using FlowJo analysis software (Tree Star Inc). Western blotting for EBV latency-associated antigens was performed using previously described antibodies (5).

Quantification of EBV viral loads by qPCR. Splenic EBV viral DNA load was quantified by real-time PCR using a Taqman PCR kit (Applied Biosystems) and a sequence detector (BioRad MyQ5). DNA was extracted using Tissue and Blood DNA kit (QIAGEN) according to the manufacturer's protocol. A region from the *Bam*HI W fragment of EBV was amplified using primers 5′-GGACCACTGCCCCTGGTATAA-3′ and 5′-TTTGTGTGGACTCCTGGGG-3′ and detected with the fluorogenic probe 5′-(FAM)-TCCTGCAGCTATTTCTGGTCGCATCA-(TAMRA)-3′. The human *BCL2* gene was amplified using primers 5′-CCTGCCCTCCTTCCGC-3′ and 5′-TGCATTTCAGGAAGACCCTGA-3′ and detected with the fluorogenic probe 5′-(FAM)-CTTTCTCATGGCTGTCC-(TAMRA)-3′. The EBV *Bam*HI W fragment copy number per cell line was calculated as $2 \times w/b$, where w is the EBV *Bam*HI W copy number and b is the *BCL2* copy number. All samples were tested in triplicate.

qPCR for gene expression. *CXCL10* mRNA quantitation (Figure 7A) was achieved from cDNA generated using GoScript reverse transcriptase (Promega). cDNA was used as a template for qPCR on a BioRad MyIQ5 detection system with Platinum Quantitative PCR SuperMix-UDG (Invitrogen). Primers used for quantification of CXCL10 were 5′-CCTGCAAGCCAATTTTGTCCACGTGTT-3′ and 5′-AGCACTGCATCGATTTTGCTCCCCTC-3′. Expression levels of *CXCL10* were normalized to the expression of *GAPDH*. *GAPDH*-detecting primers were 5′-ATGGGGAAGGTGSSGGTCG-3′ and 5′-GGGTCATTGATGGCAACAATATC-3′.

For all other gene expression analyses, 1 μg of RNA isolated using RNeasy mini kit was converted to cDNA using Superscript III reverse transcriptase (Invitrogen). Gene panels were assembled on Taqman low-density array cards, and 3–5 μl cDNA in Taqman Gene Expression mastermix (Applied Biosystems) was analyzed per lane. Relative transcript level was calculated as $2^{(40-Ct\ value)}$ and multiplied by the normalization factor for 5 endogenous control genes generated by qBase Plus (Biogazelle). This relative expression level was $\log_2$ transformed, and then average expression level for each assay was subtracted to display deviation from the mean for ease of comparison/visualization (Figure 4A and Supplemental Figure 3). Assay IDs and control assays are listed in Supplemental Table 2.

Sequencing EBNA3B from sLCLs and from frozen and formalin-fixed paraffin-embedded tumor material. DNA was extracted from archival formalin-fixed, paraffin-embedded (FFPE) EBV-positive DLBCL biopsies collected in either the United Kingdom or Australia. 2 of the Australian DLBCLs (GC-DL44 and ABC-DL67) had not been fixed prior to DNA extraction. DNA extracted from the HLs, BLs, and sLCLs was also unfixed. The BL DNA samples were described previously (53). sLCLs were grown out from peripheral blood samples from a variety of individuals, many of which were taken at primary presentation of an underlying EBV-associated disease, ranging from nasopharyngeal carcinoma (sLCL-NPC#), BL (sLCL03 and sLCL20), EBV-positive lesions associated with transplant immunosuppression (sLCL-IS#), and infectious mononucleosis (sLCL-IM#), as described in Supplemental Table 3. DNA from African sLCLs was provided by A. Rickinson, D. Croom-Carter, and J. Arrand (University of Birmingham, Birmingham, United Kingdom).

EBNA3B was amplified from the DNA samples using a set of overlapping PCR assays (Supplemental Figure 5A). Due to the short amplicon length (<300 bp) and the large number of polymorphisms between type 1 and type 2 EBV strains, different PCR assays were required for amplifying and sequencing EBNA3B from FFPE DNA from type 1 and type 2 EBV strains. Unfixed DNA was amplified using a universal primer set, although the 1980-2802 PCR assay did not reliably amplify type 2 EBV sequence and was therefore replaced by a type 2–specific PCR in some cases (data not shown).

DNA was extracted from FFPE lymphoma biopsies using the QIAamp DNA FFPE tissue kit (Qiagen), from frozen HL biopsies using the QIAamp DNA mini kit, and from LCLs by proteinase K digestion followed by phenol chloroform extraction or using the QIAamp DNA blood mini kit (Qiagen). PCR amplifications were performed with 20–50 ng of this DNA per 15-μl reaction using the HotStarPlusTaq Master Mix kit (Qiagen) for 39 cycles using an annealing temperature of 58°C. FFPE DNA was assessed for DNA integrity using a multiplex of PCR amplicons 100–400 bp in length, as previously described (54). Additionally, EBNA2 and EBNA3B types (i.e., type 1 or type 2 EBV sequence) were determined using previously described PCR assays (55). Overlapping PCR primer pairs (see Supplemental Figure 5A and Supplemental Table 4) were designed using Visual OMP (DNA Software Inc.). Smaller PCR products were prepared for sequencing by ExoSAP treatment. Specifically, 10 μl PCR product was incubated with 4 μl ExoSAP (composed of 0.2 U/μl exonuclease I and 0.5 U/μl antarctic phosphatase in 1× antarctic phosphatase buffer; all from NEB) for 20 minutes, then heat inactivated at 80°C for 15 minutes. Longer PCR products were first cleaned up using the QIAquick PCR purification kit (Qiagen). 1–8 μl of this was then used in conventional dye terminator sequencing reactions (1 reaction for each of the forward and reverse primers). DNA sequences were manually screened for base calling accuracy. Sequences were compiled into contigs using Contig Express, and contigs were aligned using AlignX, both components of Vector NTI Suite (version 11.5; Invitrogen). DNA sequence phylogeny was performed using Mega (version 5.05; ref. 56).

Statistics. Statistical significance was calculated using paired (Supplemental Figure 1) and unpaired (all other figures) 2-tailed Student's *t* test. LCLs generated from the same donor were treated as pairs. For all experiments, *P* values less than 0.05 were considered statistically significant. Differential regulation of genes by microarray analysis, and its confirmation by qPCR, was determined by 2-way ANOVA, combining host cell genetic background and virus type as factors, as described previously (5). 3-dimensional principal component analysis of qPCR data was performed on mean-normalized, $\log_2$-transformed qPCR expression values using Partek Genomic Suite (Partek Inc.).

Study approval. All animal protocols were approved by the cantonal veterinary office of the canton of Zürich, Switzerland (protocol nos. 116/2008 and 148/2011). All studies involving human samples were reviewed and approved by the cantonal ethical committee of Zürich, Switzerland (protocol no. KEK-StV-Nr.19/08). Lymphocyte concentrates were obtained from Blutspendedienst Zürich after informed consent of the donors.

Ethical approval for research with human lymphomas was given as follows. HL samples were collected with informed consent and released by the Children's Cancer and Leukemia Group (CCLG; study no. 2007 BS07; Leicester, United Kingdom), and the study was approved by the Coventry Research Ethics Committee (protocol no. 08/H1210/142; Coventry, United Kingdom). BL samples were collected in Malawi and Uganda between 1996 and 2007. Written informed consent for research use of the samples was obtained from the patients' guardians at the time of collection; this was approved by the Medical Ethical Committee of the VU University medical center (Amsterdam, The Netherlands), according to the code for proper secondary use of human tissue of the Dutch Federation of Biomedical Scientific Societies (http://www.federa.org).

Analysis of DLBCL biopsies with informed consent was approved by East London and the City HA Local Research Ethics Committee 3 (protocol no. 05/Q0605/140, identifiers 1B, 3, 4, and 7a; London, United Kingdom). Analysis of archival diagnostic biopsies from EBV-positive DLBCLs with sample identifiers starting DL or PDL was approved by the Queensland Institute of Medical Research Ethics Committee (protocol no. P1075; Brisbane, Australia), and for the other DLBCLs by National Research Ethics Service (NRES) Committee London – West London (protocol no. 09/H0707/61; London, United Kingdom). A waiver of informed consent was approved for these in order to prevent any distress to relatives of deceased patients. Establishment of cell line TRL595 from cells removed during therapeutic lymph node clearance was approved by the Institutional Review Board for Human Subject Research for Baylor College of Medicine and Affiliated Hospitals (BCM IRB; Houston, Texas, USA).

Acknowledgments

This work was supported by the Wellcome Trust (program grant 077489) to M.J. Allday and by grants from the National Cancer Institute (R01CA108609), the Sassella Foundation (10/02), Cancer Research Switzerland (KFS-02652-08-2010), the Association for International Cancer Research (11-0516), the Vontobel Foundation, Novartis, and the Swiss National Science Foundation (310030_126995) to C. Münz. P.C. Rämer is supported by a junior research fellowship from the University of Zürich. We thank Alan Rickinson, Debbie Croom-Carter, and John Arrand for provision of DNA from African sLCLs. We are grateful to Leukaemia and Lymphoma Research and to the UK Children's Cancer and Leukaemia Group for support toward the collection of HL samples.

Received for publication March 18, 2011, and accepted in revised form January 25, 2012.

Address correspondence to: Martin Allday, Section of Virology, Imperial College School of Medicine, St. Mary's Campus, Norfolk Place, London W2 1PG, United Kingdom. Phone: 44.0.207.594.3836; Fax: 44.0.207.594.3973; E-mail: m.allday@imperial.ac.uk. Or to: Christian Münz, Viral Immunobiology, Institute of Experimental Immunology, University of Zürich, Winterthurerstrasse 190, CH-8057 Zürich, Switzerland. Phone: 41.44.635.3716; Fax: 41.44.635.6883; E-mail: muenzc@immunology.uzh.ch.

1. Young LS, Rickinson AB. Epstein-Barr virus:40 years on. *Nat Rev Cancer*. 2004;4(10):757–768.
2. Cohen JI, Fauci AS, Varmus H, Nabel GJ. Epstein-barr virus: an important vaccine target for cancer prevention. *Sci Transl Med*. 2011;3(107):107fs7.
3. Thorley-Lawson DA. Epstein-Barr virus: exploiting the immune system. *Nat Rev Immunol*. 2001;1(1):75–82.
4. Küppers R. B cells under influence: transformation of B cells by Epstein-Barr virus. *Nat Rev Immunol*. 2003;3(10):801–812.
5. White RE, Groves IJ, Turro E, Yee J, Kremmer E, Allday MJ. Extensive Co-Operation between the Epstein-Barr Virus EBNA3 Proteins in the Manipulation of Host Gene Expression and Epigenetic Chromatin Modification. *PLoS ONE*. 2010;5(11):e13979.
6. Hertle ML, et al. Differential gene expression patterns of EBV infected EBNA-3A positive and negative human B lymphocytes. *PLoS Pathog*. 2009;5(7):e1000506.
7. Zhao B, et al. Epstein-Barr virus nuclear antigen 3C regulated genes in lymphoblastoid cell lines. *Proc Natl Acad Sci U S A*. 2011;108(1):337–342.
8. Anderton E, Yee J, Smith P, Crook T, White RE, Allday MJ. Two Epstein-Barr virus (EBV) oncoproteins cooperate to repress expression of the proapoptotic tumour-suppressor Bim: clues to the pathogenesis of Burkitt's lymphoma. *Oncogene*. 2008;27(4):421–433.
9. Vereide DT, Sugden B. Lymphomas differ in their dependence on Epstein-Barr virus. *Blood*. 2011;117(6):1977–1985.
10. Skalska L, White RE, Franz M, Ruhmann M, Allday MJ. Epigenetic repression of p16(INK4A) by latent Epstein-Barr virus requires the interaction of EBNA3A and EBNA3C with CtBP. *PLoS Pathog*. 2010;6(6):e1000951.
11. Maruo S, Zhao B, Johannsen E, Kieff E, Zou J, Takada K. Epstein-Barr virus nuclear antigens 3C and 3A maintain lymphoblastoid cell growth by repressing p16INK4A and p14ARF expression. *Proc Natl Acad Sci U S A*. 2011;108(5):1919–1924.
12. Allday M. How does Epstein-Barr virus (EBV) complement the activation of Myc in the pathogenesis of Burkitt's lymphoma? *Semin Cancer Biol*. 2009;19(6):366–376.
13. Nikitin PA, et al. An ATM/Chk2-mediated DNA damage-responsive signaling pathway suppresses Epstein-Barr virus transformation of primary human B cells. *Cell Host Microbe*. 2010;8(6):510–522.
14. Tomkinson B, Kieff E. Use of second-site homologous recombination to demonstrate that Epstein-Barr virus nuclear protein 3B is not important for lymphocyte infection or growth transformation in vitro. *J Virol*. 1992;66(5):2893–2903.
15. Gottschalk S, Rooney CM, Heslop HE. Post-transplant lymphoproliferative disorders. *Annu Rev Med*. 2005;56:29–44.
16. Hislop AD, Taylor GS, Sauce D, Rickinson AB. Cellular responses to viral infection in humans: lessons from Epstein-Barr virus. *Annu Rev Immunol*. 2007;25:587–617.
17. Murray RJ, et al. Identification of target antigens for the human cytotoxic T cell response to Epstein-Barr virus (EBV): implications for the immune control of EBV-positive malignancies. *J Exp Med*. 1992;176(1):157–168.
18. Khanna R, et al. Localization of Epstein-Barr virus cytotoxic T cell epitopes using recombinant vaccinia: implications for vaccine development. *J Exp Med*. 1992;176(1):169–176.
19. Münz C, et al. Human CD4(+) T lymphocytes consistently respond to the latent Epstein-Barr virus nuclear antigen EBNA1. *J Exp Med*. 2000;191(10):1649–1660.
20. Leen A, et al. Differential immunogenicity of Epstein-Barr virus latent-cycle proteins for human CD4(+) T-helper 1 responses. *J Virol*. 2001;75(18):8649–8659.
21. Strowig T, et al. Priming of protective T cell responses against virus-induced tumors in mice with human immune system components. *J Exp Med*. 2009;206(6):1423–1434.
22. Ishikawa F, et al. Development of functional human blood and immune systems in NOD/SCID/IL2 receptor {gamma} chain(null) mice. *Blood*. 2005;106(5):1565–1573.
23. Traggiai E, et al. Development of a human adaptive immune system in cord blood cell-transplanted mice. *Science*. 2004;304(5667):104–107.
24. Yajima M, et al. A new humanized mouse model of Epstein-Barr virus infection that reproduces persistent infection, lymphoproliferative disorder, and cell-mediated and humoral immune responses. *J Infect Dis*. 2008;198(5):673–682.
25. Dirmeier U, Neuhierl B, Kilger E, Reisbach G, Sandberg ML, Hammerschmidt W. Latent membrane protein 1 is critical for efficient growth transformation of human B cells by Epstein-Barr virus. *Cancer Res*. 2003;63(11):2982–2989.
26. Gottschalk S, et al. An Epstein-Barr virus deletion

mutant associated with fatal lymphoproliferative disease unresponsive to therapy with virus-specific CTLs. *Blood*. 2001;97(4):835–843.
27. Midgley RS, Bell AI, McGeoch DJ, Rickinson AB. Latent gene sequencing reveals familial relationships among Chinese Epstein-Barr virus strains and evidence for positive selection of A11 epitope changes. *J Virol*. 2003;77(21):11517–11530.
28. Görzer I, Niesters HGM, Cornelissen JJ, Puchhammer-Stöckl E. Characterization of Epstein-Barr virus Type I variants based on linked polymorphism among EBNA3A, -3B, and -3C genes. *Virus Res*. 2006;118(1–2):105–114.
29. Nguyen-Van D, et al. Epstein-Barr virus-positive diffuse large B-cell lymphoma of the elderly expresses EBNA3A with conserved CD8+ T-cell epitopes. *Am J Blood Res*. 2011;1(2):146–159.
30. Burrows JM, Khanna R, Sculley TB, Alpers MP, Moss DJ, Burrows SR. Identification of a naturally occurring recombinant Epstein-Barr virus isolate from New Guinea that encodes both type 1 and type 2 nuclear antigen sequences. *J Virol*. 1996;70(7):4829–4833.
31. Maggio EM, et al. Common and differential chemokine expression patterns in rs cells of NLP, EBV positive and negative classical Hodgkin lymphomas. *Int J Cancer*. 2002;99(5):665–672.
32. Dufour JH, Dziejman M, Liu MT, Leung JH, Lane TE, Luster AD. IFN-gamma-inducible protein 10 (IP-10; CXCL10)-deficient mice reveal a role for IP-10 in effector T cell generation and trafficking. *J Immunol*. 2002;168(7):3195–3204.
33. Luster AD, Unkeless JC, Ravetch JV. Gamma-interferon transcriptionally regulates an early-response gene containing homology to platelet proteins. *Nature*. 1985;315(6021):672–676.
34. Mlecnik B, et al. Biomolecular network reconstruction identifies T-cell homing factors associated with survival in colorectal cancer. *Gastroenterology*. 2010;138(4):1429–1440.
35. Subklewe M, Paludan C, Tsang ML, Mahnke K, Steinman RM, Münz C. Dendritic cells cross-present latency gene products from Epstein-Barr virus-transformed B cells and expand tumor-reactive CD8(+) killer T cells. *J Exp Med*. 2001;193(3):405–411.
36. Paludan C, et al. Epstein-Barr nuclear antigen 1-specific CD4(+) Th1 cells kill Burkitt's lymphoma cells. *J Immunol*. 2002;169(3):1593–1603.
37. Bickham K, et al. Dendritic cells initiate immune control of Epstein-Barr virus transformation of B lymphocytes in vitro. *J Exp Med*. 2003;198(11):1653–1663.
38. Pule MA, et al. Virus-specific T cells engineered to coexpress tumor-specific receptors: persistence and antitumor activity in individuals with neuroblastoma. *Nat Med*. 2008;14(11):1264–1270.
39. Isaksson A, Berggren M, Ricksten A. Epstein-Barr virus U leader exon contains an internal ribosome entry site. *Oncogene*. 2003;22(4):572–581.
40. Aitken C, Sengupta SK, Aedes C, Moss DJ, Sculley TB. Heterogeneity within the Epstein-Barr virus nuclear antigen 2 gene in different strains of Epstein-Barr virus. *J Gen Virol*. 1994;75(pt 1):95–100.
41. Kelly G, Bell A, Rickinson A. Epstein-Barr virus-associated Burkitt lymphomagenesis selects for downregulation of the nuclear antigen EBNA2. *Nat Med*. 2002;8(10):1098–1104.
42. Deacon EM, et al. Epstein-Barr virus and Hodgkin's disease: transcriptional analysis of virus latency in the malignant cells. *J Exp Med*. 1993; 177(2):339–349.
43. Rooney CM, et al. Use of gene-modified virus-specific T lymphocytes to control Epstein-Barr-virus-related lymphoproliferation. *Lancet*. 1995; 345(8941):9–13.
44. Campeau E, et al. A versatile viral system for expression and depletion of proteins in mammalian cells. *PLoS One*. 2009;4(8):e6529.
45. Schmid D, Pypaert M, Münz C. Antigen-loading compartments for major histocompatibility complex class II molecules continuously receive input from autophagosomes. *Immunity*. 2007;26(1):79–92.
46. Strowig T, et al. Human NK cells of mice with reconstituted human immune system components require preactivation to acquire functional competence. *Blood*. 2010;116(20):4158–4167.
47. Gurer C, et al. Targeting the nuclear antigen 1 of Epstein-Barr virus to the human endocytic receptor DEC-205 stimulates protective T-cell responses. *Blood*. 2008;112(4):1231–1239.
48. Lacerda JF, Ladanyi M, Louie DC, Fernandez JM, Papadopoulos EB, O'Reilly RJ. Human Epstein-Barr virus (EBV)-specific cytotoxic T lymphocytes home preferentially to and induce selective regressions of autologous EBV-induced B cell lymphoproliferations in xenografted C.B-17 scid/scid mice. *J Exp Med*. 1996;183(3):1215–1228.
49. Subklewe M, et al. Dendritic cells expand Epstein Barr virus specific CD8+ T cell responses more efficiently than EBV transformed B cells. *Hum Immunol*. 2005;66(9):938–949.
50. Ferlazzo G, et al. The abundant NK cells in human secondary lymphoid tissues require activation to express killer cell Ig-like receptors and become cytolytic. *J Immunol*. 2004;172(3):1455–1462.
51. Smith CA, et al. Production of genetically modified Epstein-Barr virus-specific cytotoxic T cells for adoptive transfer to patients at high risk of EBV-associated lymphoproliferative disease. *J Hematother*. 1995;4(2):73–79.
52. Spies T, et al. A gene in the human major histocompatibility complex class II region controlling the class I antigen presentation pathway. *Nature*. 1990;348(6303):744–747.
53. Paschos K, Smith P, Anderton E, Middeldorp JM, White RE, Allday MJ. Epstein-Barr virus latency in B cells leads to epigenetic repression and CpG methylation of the tumour suppressor gene Bim. *PLoS Pathog*. 2009;5(6):e1000492.
54. van Dongen JJM, et al. Design and standardization of PCR primers and protocols for detection of clonal immunoglobulin and T-cell receptor gene recombinations in suspect lymphoproliferations: report of the BIOMED-2 Concerted Action BMH4-CT98-3936. *Leukemia*. 2003;17(12):2257–2317.
55. Sample J, et al. Epstein-Barr virus types 1 and 2 differ in their EBNA-3A, EBNA-3B, and EBNA-3C genes. *J Virol*. 1990;64(9):4084–4092.
56. Tamura K, Peterson D, Peterson N, Stecher G, Nei M, Kumar S. MEGA5: molecular evolutionary genetics analysis using maximum likelihood, evolutionary distance, and maximum parsimony methods. *Mol Biol Evol*. 2011;28(10):2731–2739.